

Search for Heavy Neutral Leptons with IceCube DeepCore

Dissertation
zur Erlangung des akademischen Grades
doctor rerum naturalium
(Dr. rer. nat.)

im Fach: Physik
Spezialisierung: Experimentalphysik

eingereicht an der
Mathematisch-Naturwissenschaftlichen Fakultät
der Humboldt-Universität zu Berlin

von
Leander Fischer M. Sc.
geboren am 24. Oktober 1992
in Heidelberg

Präsidentin der Humboldt-Universität zu Berlin
Prof. Dr. Julia von Blumenthal

Dekanin der Mathematisch-Naturwissenschaftlichen Fakultät
Prof. Dr. Caren Tischendorf

Copyright Notice

This book is released into the public domain using the CC-BY-4.0 code.

To view a copy of the CC-BY-4.0 code, visit:

<https://creativecommons.org/licenses/by/4.0/>

Colophon

This document was typeset with the help of KOMA-Script and L^AT_EX using the open-source kaobook template class.

The source code of this thesis is available at:

https://github.com/LeanderFischer/phd_thesis

Zusammenfassung

Zusammenfassung ...

Abstract

Abstract ...

Todo list

Also cite this? Didn't find a good reference, only the press releases.	1
Introduce SM EW NC/CC Lagrangian to build upon in the next chapter	3
Cite and/or sidenote this.	3
cite this	3
cite neutrino oscillations/flavor conversions	4
Re-write/re-formulate this section (copied from HNL technote).	5
Produce similar styled plot for these limits	5
This section really needs to be re-written to motivate the search for HNLs from a more generic point of view (e.g. to explain neutrino masses)	6
This section definitely needs to be elaborated in a little more detail	6
Not adding information about the case where the neutrinos have Dirac or pseudo-Dirac masses	7
(Re-)write for PhD thesis (just copy paste from M.Sc.).	9
Plot is missing + for W and 0 for Z boson.	9
SB: It seems that you have some double counting of information here . I suggest to move some of the information in this "intro" paragraph to the appropriate subsections	10
Explain momenta and momentum transfer (p,q) in these figures.	11
(Re-)write BSM chapter for PhD thesis (just copy paste from M.Sc.).	11
SB: You could say why with an extra half-sentence.	12
SB: I don't think this is true - the normalization is known to 5% if you trust Anatoli/Juan Pablo. Please have a look at more recent publications on this topic.	12
SB: formatting/margins also I don't think you defined $\rho_{1,2}$	12
add fancy icecube picture	15
SB: there are more properties than just these. Somehow need a half sentence that explains why these are particularly important to single out (see ice papers for inspiration)	16
CL: maybe define that absorption and scattering lengths are? they are defined differently so this invites a comparison that is not so obvious	16
Add reference for the dust layer!	16
exchange for figure with scattering (check abs/sca is correct)	16
mention/cite dust logger paper/procedure?	16
Add accuracy of the efficiency calibration here.	17
Maybe throw the coordinate system in a box on the side?	17
Blow up this image a bit, so it's better readable as marginfigure.	17
CL: value?	18

SB: this needs revision. the energy range you mention is particular for oscillations already (atmopsheric neutrinos are plentiful outside of this range you mentioned). If you rewrite the first part you'll have to revisit the second part. Also in general I'd suggest not to rank analyses like Main and Other - DeepCore was orginally intended as a dark matter detector, and there are probably more DM analyses unblinded / year than oscillations. Just keep it general, no need to rank.	18
Cite n and θ_c	18
SB: you already mentioned that Cher. Rad. doesn't lead to significant energy loss. I suggest to clean up the text a bit, you dont' need to emphasize that so many times. Pick one place (probably here) and eliminate it elsewhere	19
Add reference (PDG or find original)	19
SB: i like that you give a benchmark value here, for rule of thumb or so, but it should be related to the detector geometry somehow or else it feels too out of place. Give it some context	19
Add reference for these processes.	20
cite em shower distribution	20
Add angular profile plot (Summer agrees!) (create one based on Leif Rädel as Alex did)	20
SB: rephrase gamma (from equation) is not defined	20
SB: Explain	21
Make sure I have this defined in the SM interaction chapter!	22
SB: Since your analysis depends on the ability to reconstruct cascade directions, it seems odd to emphasize that the light is nearly isotropically emitted. Of course that is true, but the emphasis should rather be on the fact that there remains some assymetry to the light profile	22
Adapt to reflect switched chapter order	23
Make my own DC string positions/distances plot version.	24
Re-make plot with all energies (cascades and total, both sets (they are the same))	25
Re-make plot with all decay lengths (both sets)	25
Re-make plot with 3 target masses and better labels	28
Add comparions of SM cross-sections between NuXSSplMkr and genie?	29
add varied total cross-section for a few background HNL events (for QE/RES variations?!?)	29
Calculate max BRs	29
JVS: consider also writing down the (trivial) 2-body decay kinematics for completeness and consistency. This transition is a bit jarring as it is	30
add table with number of gen level files? mention the event number is smaller becasue of kinematic condition?	32
Re-make plot with x,y for horizontal set one plot!	37
Re-make plot with x, y, z for both cascades in one.	37
Re-arrange plots in a more sensible way.	37

Contents

Abstract	iii
Contents	vii
1 Standard Model Neutrinos and Beyond	1
1.1 The Standard Model	1
1.1.1 Fundamental Fields	1
1.1.2 Electroweak Symmetry Breaking	2
1.1.3 Fermion Masses	3
1.1.4 Weak Interactions after Symmetry-Breaking	3
1.2 Evidence for Beyond Standard Model Physics	3
1.3 Beyond Standard Model Neutrinos	4
1.3.1 Mass Mechanisms	4
1.3.2 A Solution to (some of) the Problems	5
1.3.3 The Minimal Standard Model Extension	6
1.3.4 Existing Constraints on Heavy Neutral Leptons	8
1.4 Atmospheric Neutrinos	9
1.4.1 Oscillations	11
1.4.2 Heavy Neutral Lepton Production and Decay in IceCube DeepCore	13
2 The IceCube Neutrino Observatory	15
2.1 Detector Components	15
2.1.1 Digital Optical Modules and the Antarctic Ice	16
2.1.2 IceCube	17
2.1.3 DeepCore	17
2.2 Particle Propagation in Ice	18
2.2.1 Cherenkov Effect	18
2.2.2 Energy Losses	19
2.3 Event Morphologies	21
3 Heavy Neutral Lepton Signal Simulation	23
3.1 Model Independent Simulation	23
3.1.1 Generator Functions	23
3.1.2 Simplistic Sets	24
3.1.3 Realistic Set	26
3.2 Model Dependent Simulation	27
3.2.1 Custom LeptonInjector	27
3.2.2 Sampling Distributions	31
3.2.3 Weighting Scheme	31
3.2.4 Generation Level Distributions	32
APPENDIX	35
A Heavy Neutral Lepton Signal Simulation	37
A.1 Model Independent Simulation Distributions	37
A.2 Model Dependent Simulation Distributions	38
B Analysis Checks	39
B.1 Minimization Robustness	39
B.1.1 Ensemble Tests	39

List of Figures

1.1 Current $ U_{\tau 4}^2 - m_4$ limits	5
1.2 Feynman diagram of HNL up-scattering process	7
1.3 Feynman diagram of HNL decay	8
1.4 HNL branching ratios	8
1.5 HNL decay widths	9
1.6 Feynman diagrams of neutrino weak interactions	9
1.7 Total inclusive neutrino-nucleon cross-sections	10
1.8 Neutrino-nucleon deep inelastic scattering	11
1.9 Atmospheric neutrino fluxes	12
2.1 IceCube overview	15
2.2 IceCube sideview	16
2.3 Digital Optical Module (DOM)	17
2.4 IceCube top view	17
2.5 Cherenkov light front	18
3.1 DeepCore string spacing	24
3.2 Simplified model independent simulation generation level distributions	25
3.3 Realistic model independent simulation generation level distributions	27
3.4 HNL branching ratios	28
3.5 Custom HNL total cross-sections for the four target masses compared to the total ($\nu_\tau/\bar{\nu}_\tau$ NC) cross-section used for SM neutrino simulation production with GENIE.	29
3.6 Model dependent simulation generation level distributions	33
A.1 Simplified model independent simulation generation level distributions	37
A.2 Realistic model independent simulation generation level distributions	38
A.3 Model dependent simulation generation level distributions	38
B.1 Asimov inject/recover test (0.3 GeV, 1.0 GeV)	39
B.2 Pseudo-data trials TS distribution (0.3 GeV, 1.0 GeV)	39

List of Tables

1.1	Standard model fermions	2
2.1	IceCube low energy event signatures and underlying interactions	21
3.1	Simplified model independent simulation sampling distributions	25
3.2	Realistic model independent simulation sampling distributions	26
3.3	HNL mass dependent decay channels	29
3.4	Model dependent simulation sampling distributions	31

Standard Model Neutrinos and Beyond

1

1.1 The Standard Model

The *Standard Model (SM)* of particle physics is a Yang-Mills theory [1] providing very accurate predictions of weak, strong, and *electromagnetic (EM)* interactions. It is a relativistic quantum field theory that relies on gauge invariance, where all matter is made up of fermions, which are divided into quarks and leptons, and bosons describe the interactions between the fermions that have to fulfil the overall symmetry of the theory. Leptons are excitations of Dirac-type fermion fields.

The initial idea of the theory is associated with the works of Weinberg [2], Glashow [3], and Salam [4], that proposed a unified description of EM and weak interactions as a theory of a spontaneously broken $SU(2) \times U(1)$ symmetry for leptons, predicting a neutral massive vector boson Z^0 , a massive charged vector boson W^\pm , and a massless photon γ as the gauge bosons. The Higgs mechanism [5], describing the breaking of the symmetry, predicts the existence of an additional scalar particle, the Higgs boson, giving the W^\pm and Z^0 bosons their mass. The Higgs boson was discovered in 2012 at the LHC.

Gell-Mann and Zweig proposed the quark model in 1964 [6, 7], which was completed by the discovery of non-abelian gauge theories [8] to form the $SU(3)$ symmetry of the strong interaction called *quantum chromodynamics (QCD)*. QCD describes the interaction between quarks and gluons which completed the full picture of the SM in the mid-1970s. Together with the electroweak theory, the SM is a $SU(3)_C \times SU(2)_L \times U(1)_Y$ local gauge symmetry, with the conserved quantities C , *color*, L , *left-handed chirality*, and Y , *weak hypercharge*.

In the following, the basic properties of the SM are described, following the derivations of [9, 10].

1.1.1 Fundamental Fields

Fermions in the SM are Weyl fields with either *left-handed (LH)* or *right-handed (RH)* chirality, meaning they are eigenvectors of the chirality operator γ_5 with $\gamma_5\psi_{R/L} = \pm\psi_{R/L}$. Only LH particles transform under $SU(2)_L$. The Higgs field is a complex scalar field, a doublet of $SU(2)_L$, which is responsible for the spontaneous symmetry breaking of $SU(2)_L \times U(1)_Y$ to $U(1)_{\text{EM}}$. Local gauge transformations of the fields are given by

$$\psi \rightarrow e^{ig\theta^a(x)T^a} \psi , \quad (1.1)$$

where g is the coupling constant, $\theta^a(x)$ are the parameters of the transformation, and T^a are the generators of the group, with a counting them. The number of bosons is dependent on the generators of the symmetry groups, while the strength is defined by the coupling constants. There are eight massless gluons corresponding to the generators of the $SU(3)_C$

1.1 The Standard Model	1
1.2 Evidence for Beyond Standard Model Physics	3
1.3 Beyond Standard Model Neutrinos	4
1.4 Atmospheric Neutrinos	8
Isotopic Spin and Isotopic Gauge Invariance"	

[2]: Weinberg (1967), "A Model of Leptons"

[3]: Glashow (1961), "Partial-symmetries of weak interactions"

[5]: Higgs (1964), "Broken symmetries, massless particles and gauge fields"

Also cite this? Didn't find a good reference, only the press releases.

[6]: Gell-Mann (1964), "A Schematic Model of Baryons and Mesons"

[7]: Zweig (1964), "An $SU(3)$ model for strong interaction symmetry and its breaking. Version 2"

[9]: Giunti et al. (2007), *Fundamentals of Neutrino Physics and Astrophysics*

[10]: Schwartz (2013), *Quantum Field Theory and the Standard Model*

group. These mediate the strong force which conserves color charge. The W_1, W_2, W_3 , and B boson fields of the $SU(2)_L \times U(1)_Y$ group are mixed into the massive bosons through spontaneous symmetry breaking as

$$W^\pm = \frac{1}{\sqrt{2}}(W_1 \mp iW_2) \quad (1.2)$$

and

$$Z^0 = \cos \theta_W W_3 - \sin \theta_W B, \quad (1.3)$$

with θ_W being the *Weinberg angle*. The massless photon field is given by

$$A = \sin \theta_W W_3 + \cos \theta_W B \quad (1.4)$$

and its conserved quantity is the EM charge Q , which depends on the weak hypercharge, Y , and the third component of the weak isospin, T_3 , as $Q = T_3 + Y/2$.

	Type			Q
quarks	u	c	t	+2/3
	d	s	b	-1/3
leptons	ν_e	ν_μ	ν_τ	0
	e	μ	τ	-1

Table 1.1: Fermions in the Standard Model. Shown are all three generations of quarks and leptons with their electric charge Q .

Fermions are divided into six quarks and six leptons. Weak, strong, and EM force act on the quarks, and they are always found in bound form as baryons or mesons. Leptons do not participate in the strong interaction and only the electrically charged leptons are massive and are effected by the EM force, while neutrinos are massless and only interact via the weak force. Each charged lepton has an associated neutrino, which it interacts with in *charged-current (CC)* weak interactions, that will be explained in more detail in Section 1.1.4. The fermions are listed in Table 1.1.

1.1.2 Electroweak Symmetry Breaking

To elaborate the process of spontaneous symmetry breaking through which the gauge bosons of the weak interaction acquire their masses, the Lagrangian of the Higgs field is considered as

$$\mathcal{L}_{\text{Higgs}} = (D_\mu \Phi^\dagger)(D^\mu \Phi) - \lambda \left(\Phi^\dagger \Phi - \frac{v^2}{2} \right)^2, \quad (1.5)$$

with parameters λ and v , where λ is assumed to be positive. Φ is the Higgs doublet, which is defined as

$$\Phi = \begin{pmatrix} \Phi^+ \\ \Phi^0 \end{pmatrix}, \quad (1.6)$$

with the charged component Φ^+ and the neutral component Φ^0 . The covariant derivative is given by

$$D_\mu = \partial_\mu - ig_2 \frac{\sigma^i}{2} W_\mu^i - \frac{1}{2}ig_1 B_\mu, \quad (1.7)$$

with the Pauli matrices σ^i and the gauge boson fields W_μ^i and B_μ of the $SU(2)_L$ and $U(1)_Y$ groups, respectively. The coupling constants g_2 and g_1 are the respective coupling constants which are related to the Weinberg angle as $\tan \theta_W = \frac{g_1}{g_2}$. The Higgs potential has a non-zero *vacuum expectation value (vev)* at the minimum of the potential at $\Phi^\dagger \Phi = \frac{v^2}{2}$. Since the vacuum is electrically neutral, it can only come from a neutral

component of the Higgs doublet as

$$\Phi_{\text{vev}} = \frac{1}{\sqrt{2}} \begin{pmatrix} 0 \\ v \end{pmatrix}. \quad (1.8)$$

1.1.3 Fermion Masses

The mass term for charged fermions with spin-1/2 is given by

$$\mathcal{L}_{\text{Dirac}} = m(\bar{\Psi}_R \Psi_L - \bar{\Psi}_L \Psi_R), \quad (1.9)$$

composed of the product of left- and RH Weyl spinors $\Psi_{L/R}$. This term is not invariant under $SU(2)_L \times U(1)_Y$ gauge transformations, but adding a Yukawa term

$$\mathcal{L}_{\text{Yukawa}} = -y \bar{L}_L \Phi e_R + \text{h.c.}, \quad (1.10)$$

coupling the fermion fields to the Higgs field, recovers the invariance and gives the fermions their masses. Here, y is the Yukawa coupling constant and \bar{L}_L is the $SU(2)_L$ doublet. With the vev, this results in the mass term for the charged leptons and down-type quarks of $-m_e(\bar{e}_L e_R + \bar{e}_R e_L)$ with $m_e = \frac{yv}{\sqrt{2}}$. With $\tilde{\Phi} = i\sigma_2 \Phi^*$, a similar Yukawa term can be written as $-y \bar{L}_L \tilde{\Phi} u_R + \text{h.c.}$, which leads to the masses of the up-type quarks.

1.1.4 Weak Interactions after Symmetry-Breaking

Introduce SM EW NC/CC Lagrangian to build upon in the next chapter

1.2 Evidence for Beyond Standard Model Physics

Are the fundamentals of the SM described above enough to explain *all* observed phenomena? Gravity cannot be explained by the SM, as it is incompatible with general relativity. Neither can the SM explain some cosmological observations like dark matter, and the matter-antimatter asymmetry, and it does not predict neutrinos to have mass, which is experimentally proven by neutrino oscillations, so some extensions to the SM is needed in order to explain them.

Cite and/or sidenote this.

Standard cosmology (Λ CDM) assumes that equal amounts of matter and anti-matter were produced in the early universe. However, the universe today is dominantly made up of matter. This so-called *baryon asymmetry* can be measured by the difference between the number densities of baryons and anti-baryons normalized to the number density of photons as

$$\eta_B = \frac{n_B - n_{\bar{B}}}{n_\gamma}, \quad (1.11)$$

where n_B , $n_{\bar{B}}$, and n_γ are the number densities of baryons, anti-baryons, and photons, respectively. Baryons are the dominant component with η_B being observed to be around 6×10^{-10} . Leptogenesis and EW baryogenesis are scenarios that could explain this phenomenon, where the former could be realized by the existence of heavy RH neutrinos.

cite this

cite neutrino oscillations/flavor conversions

The observation of neutrino flavor conversions and neutrino oscillations in a multitude of experiments is the strongest evidence for physics beyond the SM. The observation that neutrinos change their flavor while they propagate through space can only be explained, if at least two neutrinos have a non-zero mass. This is not predicted by the SM, but adding additional RH neutrinos states to the theory could explain the origin of the observed non-zero neutrino masses and could be tested for by searching for corresponding signatures in experiments.

1.3 Beyond Standard Model Neutrinos

1.3.1 Mass Mechanisms

There are no RH neutrinos in the SM and therefore the mass mechanism described in Section 1.1.3, which couples the Higgs field to LH and RH Weyl fields, predicts them to be massless. From experimental observations it is known that at least two of the three neutrino generations need to have a non-zero mass. Assuming the existence of RH neutrinos fields ν_R , one way of producing the neutrino masses is by adding a Yukawa coupling term similar to the one for up-type quarks mentioned in Section 1.1.3, to write the full Yukawa Lagrangian as

$$\mathcal{L}_{\text{Yukawa}} = -Y_{ij}^e \bar{L}_L^i \Phi e_R^j - Y_{ij}^\nu \bar{L}_L^i \tilde{\Phi} \nu_R^j + \text{h.c.}, \quad (1.12)$$

with i, j running over the three generations of leptons e, μ , and τ , and Y^e and Y^ν being the Yukawa coupling matrices. Diagonalizing the Yukawa coupling matrices through unitary transformations U^e and U^ν leads to the Dirac mass Lagrangian in the mass basis as

$$\mathcal{L}_{\text{Dirac}}^{\text{mass}} = \frac{v}{\sqrt{2}} (\bar{e}_L M_e e_R - \bar{\nu}_L M_\nu \nu_R), \quad (1.13)$$

where M_e and M_ν are the diagonal mass matrices of leptons and neutrinos, respectively.

Below here isn't quite done yet..

An additional way of generating neutrino masses is by adding a Majorana mass term of the form

$$\mathcal{L}_{\text{Majorana}} = -\frac{1}{2} M_{ij} (\nu_R^i)^c \nu_R^j + \text{h.c.}, \quad (1.14)$$

with M_{ij} being the Majorana mass matrix and the indices i, j running over all RH neutrino generations. The superscript c denotes the charge conjugate field.

$$N = \begin{pmatrix} \nu_L \\ \nu_R^c \end{pmatrix}, \quad (1.15)$$

with ν_R containing the N new RH neutrino fields.

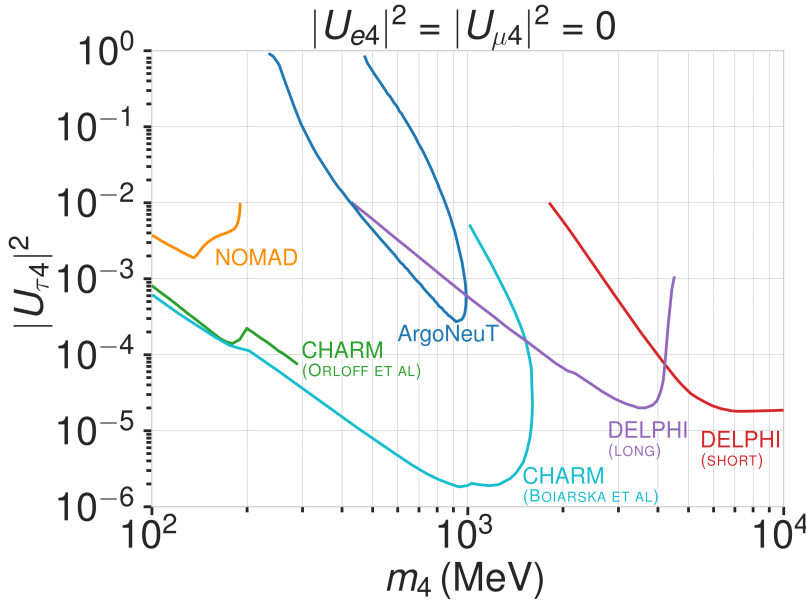


Figure 1.1: Current $|U_{\tau 4}^2| - m_4$ limits from NOMAD [12], ArgoNeut [13], CHARM [14, 15], and DELPHI [16].

The full neutrino mass Lagrangian is then given by the sum of the Dirac and Majorana mass terms as

$$\mathcal{L}_{\text{Dirac+Majorana}}^{\text{mass},\nu} = \frac{1}{2} \mathbf{N}^T \hat{C} M^{\text{D+M}} \mathbf{N} + \text{h.c.}, \quad (1.16)$$

and the mass matrix is given by

$$M^{\text{D+M}} = \begin{pmatrix} 0 & (M^D)^T \\ M^D & M^R \end{pmatrix}, \quad (1.17)$$

From AT: "Such a right-handed field would be uncharged with respect to all symmetry groups of the SM and therefore would not interact with any other particle, and hence it is called a sterile neutrino"

"It is worth noting that, in this picture of pure Dirac neutrino masses, there is no mixing between the left-handed and the right-handed states, and therefore there is no observable oscillation effect that could be measured between active and sterile neutrinos."

See-Saw Variants

Radiative Neutrino Masses

1.3.2 A Solution to (some of) the Problems

Extensions to the Standard Model (SM) that add *Heavy Neutral Leptons (HNLs)* provide a good explanation for the origin of neutrino masses through different seesaw mechanisms [11]. While the mixing with $\nu_{e/\mu}$ is strongly constrained ($|U_{\alpha 4}^2| \lesssim 10^{-5} - 10^{-8}, \alpha = e, \mu$), the mixing with ν_τ is much harder to probe due to the difficulty of producing and detecting ν_τ . Figure 1.1 shows the current limits on the τ -sterile mixing space

Re-write/re-formulate this section (copied from HNL technote).

[11]: Yanagida (1980), "Horizontal Symmetry and Masses of Neutrinos"

Produce similar styled plot for these limits

[17]: Coloma et al. (2017), “Double-Cascade Events from New Physics in Icecube”

for HNL masses between 0.1 GeV-10 GeV. As was first pointed out in [17], the atmospheric neutrino flux observed in IceCube offers a way to constrain the neutrino-HNL mixing parameters. By using the large fraction of atmospheric ν_μ events that oscillate into ν_τ before they reach the detector, the less constrained τ -sterile mixing space can be explored. In this document, we present the methodology and strategy of a search for HNLs with IceCube DeepCore. These additional RH neutrinos can be included in the Standard Model (SM) by extending the PMNS matrix to at least a 3x4 matrix as

$$\begin{pmatrix} \nu_e \\ \nu_\mu \\ \nu_\tau \\ \nu_s \end{pmatrix} = \begin{pmatrix} U_{e1} & U_{e2} & U_{e3} & U_{e4} \\ U_{\mu 1} & U_{\mu 2} & U_{\mu 3} & U_{\mu 4} \\ U_{\tau 1} & U_{\tau 2} & U_{\tau 3} & U_{\tau 4} \\ U_{s1} & U_{s2} & U_{s3} & U_{s4} \end{pmatrix} \begin{pmatrix} \nu_1 \\ \nu_2 \\ \nu_3 \\ \nu_4 \end{pmatrix}, \quad (1.18)$$

where the components with index 4 define the mixing between the flavor states and the fourth sterile mass state, respectively. Note here that this is not a theoretically fully consistent picture, but rather the phenomenologically minimal model to be tested by this analysis. This can hopefully be put into the larger context of several fully consistent models, later. Due to the singlet nature of the RH neutrinos, they only interact weakly, inheriting these interactions from their LH neutrino counterparts via mixing. This mixing of the HNLs with the electron, muon, and tau neutrinos can be probed and constrained as a function of the HNL mass by searching for their production and decay. In [17, 18] this search is mainly motivated through two experimental arguments. Secondly, IceCube is ideally placed to explore the yet unconstrained $|U_{\tau 4}|^2 - m_4$ phase-space that is not easily accessible by accelerator-based experiments.

[17]: Coloma et al. (2017), “Double-Cascade Events from New Physics in Icecube”

[18]: Coloma (2019), “Icecube/DeepCore tests for novel explanations of the Mini-BooNE anomaly”

This section really needs to be re-written to motivate the search for HNLs from a more generic point of view (e.g. to explain neutrino masses)

This section definitely needs to be elaborated in a little more detail

[19]: Coloma et al. (2021), “GeV-scale neutrinos: interactions with mesons and DUNE sensitivity”

1.3.3 The Minimal Standard Model Extension

In order to probe the τ -sterile mixing parameter, it is required to look at interactions involving τ neutrinos. However, most neutrinos produced in cosmic ray interactions with the atmosphere are ν_e or ν_μ . Therefore, we need these neutrinos to oscillate to the τ flavor before reaching the detector. For this to happen at the considered energies a traveled distance of the order of the earth diameter is necessary. This is why our signal is mostly up-going and passing through the whole earth.

To explain the signature we can observe in IceCube we first have to revisit the weak interactions that the HNL inherits from its LH counterpart through mixing. We will be following the derivation in [19]. Extending the SM by n additional RH neutrinos, ν_i ($i = 3 + n$), leads to the mass Lagrangian

$$\mathcal{L}_\nu^{\text{mass}} \supset - \sum_{\alpha=e,\mu,\tau} \sum_{i=4}^{3+n} Y_{\nu,\alpha i} \bar{L}_{L,\alpha} \tilde{\phi} \nu_i - \frac{1}{2} \sum_{i=4}^{3+n} M_i \bar{\nu}_i \nu_i^c + \text{h.c.}, \quad (1.19)$$

in a basis where the Majorana mass terms are diagonal. $Y_{\nu,\alpha i}$ are the Yukawa couplings to the lepton doublets and M the Majorana masses for the heavy singlets. $L_{L,\alpha}$ stands for the SM LH lepton doublet of flavor α while ϕ is the Higgs field, and $\tilde{\phi} = i\sigma_2\phi^*$ and $\nu_i^c \equiv C\bar{\nu}_i^t$, with $C = i\gamma_0\gamma_2$

in the Weyl representation. The full neutrino mass matrix with the Higgs vacuum expectation value $v/\sqrt{2}$ reads

$$\mathcal{M} = \begin{pmatrix} 0_{3 \times 3} & Y_\nu v / \sqrt{2} \\ Y_\nu^t v / \sqrt{2} & M \end{pmatrix}, \quad (1.20)$$

and can be diagonalized by a $(3+n) \times (3+n)$ full unitary rotation U , that itself leads to neutrino masses upon diagonalization, additionally manifesting the mixing between active neutrinos and heavy states. The resulting model consists of 3 light SM neutrino mass eigenstates ν_i ($i = 1, 2, 3$) and n heavier states, as introduced above. The flavor states will now consist of a combination of light and heavy states

$$\nu_\alpha = \sum_{i=1}^{3+n} U_{\alpha i} \nu_i, \quad (1.21)$$

and the leptonic part of the EW Lagrangian can be written as

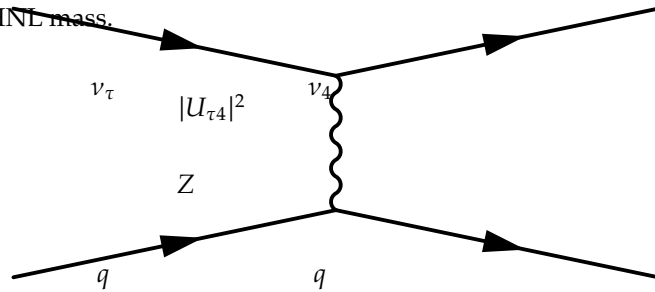
$$\begin{aligned} \mathcal{L}_{EW}^\ell = & \frac{g}{\sqrt{2}} W_\mu^+ \sum_\alpha \sum_i U_{\alpha i}^* \bar{\nu}_i \gamma^\mu P_L \ell_\alpha + \frac{g}{4c_w} Z_\mu \\ & \times \left\{ \sum_{i,j} C_{ij} \bar{\nu}_i \gamma^\mu P_L \nu_j + \sum_\alpha \bar{\ell}_\alpha \gamma^\mu [2s_w^2 P_R - (1-2s_w^2) P_L] \ell_\alpha \right\} + \text{h.c.}, \end{aligned}$$

where $c_w \equiv \cos \theta_w$, $s_w \equiv \sin \theta_w$, and θ_w the SM weak mixing angle. P_L and P_R are the left and right projectors, respectively, while

$$C_{ij} \equiv \sum_\alpha U_{\alpha i}^* U_{\alpha j}. \quad (1.22)$$

The indices now sum over all $(3+n)$ flavor and mass states.

Based on this formulation and assuming that only the mixing with the tau sector is open ($|U_{\alpha 4}^2| = 0, \alpha = e, \mu$), the relevant production diagram of the HNL can be drawn as shown in Figure 1.2. Alongside the fourth heavy mass state, a Hadronic cascade is produced. The heavy mass state will travel for some distance (dependent on mass and mixing) before it decays. The subsequent decay processes are depicted in Figure 1.3. It can be a CC or NC decay and both leptonic and mesonic modes are possible (dependent on the mass). This will produce a tau or a tau neutrino and another cascade that can be EM or Hadronic. The branching ratios corresponding to the decay modes of the HNL for the mass range of interest (i.e. between 100 MeV and 1 GeV) are shown in Figure 1.4a as a function of the HNL mass.



Not adding information about the case where the neutrinos have Dirac or pseudo-Dirac masses

Figure 1.2: Production of a sterile neutrino in the up-scattering of a tau neutrino.

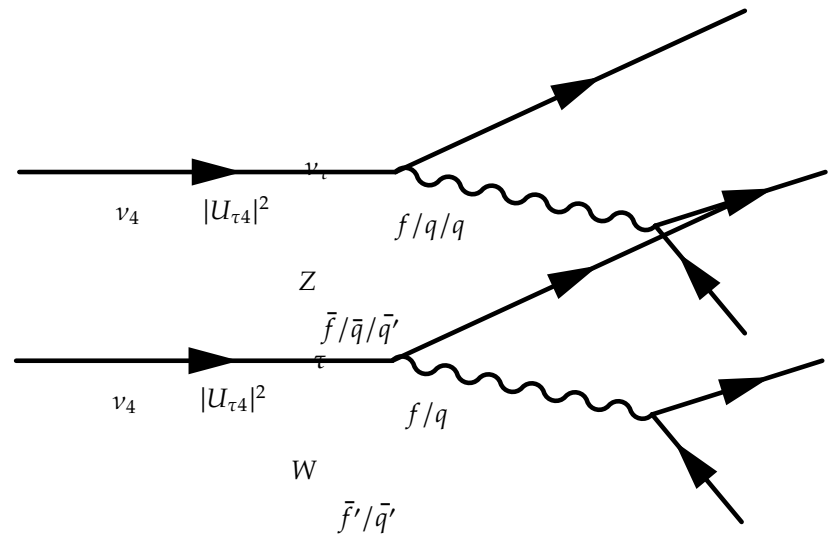


Figure 1.3: Sterile neutrino decay through neutral current (left) and charged current (right).

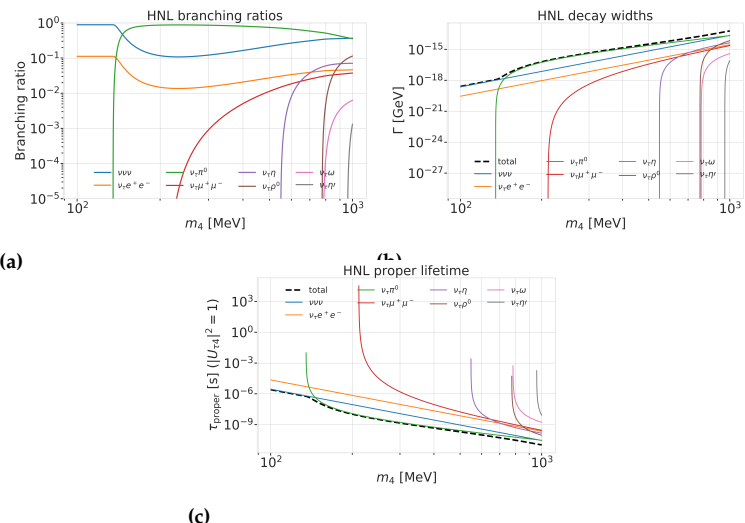


Figure 1.4: Branching ratios, decay widths, and proper lifetime of the HNL within the mass range considered, calculated based on the results from [19].

1.3.4 Existing Constraints on Heavy Neutral Leptons

xx constraints

yy constraints

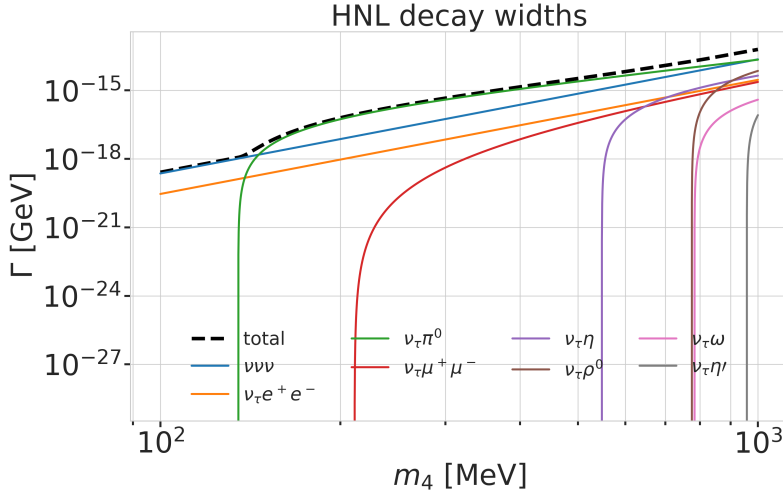


Figure 1.5: Decay widths of the HNL within the mass range considered, calculated based on the results from [19]. Given the existing constraints on $|U_{e4}|^2$ and $|U_{\mu 4}|^2$, we consider that the corresponding decay modes are negligible.

1.4 Atmospheric Neutrinos

The neutrino is an elementary particle in the SM [20]. It belongs to the class of leptons, which itself is a subclass of elementary fermions (spin $\frac{1}{2}$ particles). The fermions - six quarks and six leptons - form the matter content of the universe. Quarks take part in all three interaction types (forces) of the SM: strong, weak, and EM [21]. The charged leptons - electron, muon, and tau - are subject to the weak and the EM interaction. Neutrinos carry neither electric charge nor color charge and therefore only take part in weak interactions. There are three distinct neutrino flavors - electron neutrinos, muon neutrinos and tau neutrinos (ν_e , ν_μ , and ν_τ) [22] - each corresponding to their charged lepton counterparts.

In the SM, weak interactions are mediated by the three massive bosons W^+ , W^- , and Z^0 [20]. The large boson masses ($m_W \sim 80 \text{ GeV}$, $m_Z \sim 90 \text{ GeV}$) result in a short range of the force of about $10 \times 10^{-18} \text{ m}$. Weak interactions carried by W^\pm bosons are called CC interactions, because charge is transferred between the interacting particles. In CC interactions, a neutrino is converted into its corresponding charged lepton or vice versa. Neutral current (NC) interactions are those mediated by Z^0 bosons. Here no charge is transferred. The Feynman diagrams for CC and NC interactions are shown in Figure 1.6.

Although neutrinos are massless in the SM, we know today that they do have a small mass. The observed phenomenon of neutrino oscillations (see Section 1.4.1) is based on the fact that there is a mass difference between the three neutrino mass eigenstates. From neutrino oscillation measurements the absolute mass scale cannot be determined, since they only depend on the mass differences, but there are upper limits on the sum of all neutrino masses from cosmological observations. These upper limits are typically between 0.3 and 1.3 eV [22].

(Re-)write for PhD thesis
(just copy paste from M.Sc.).

[20]: Thomson (2013), *Modern particle physics*

[21]: Glashow (1961), "Partial-symmetries of weak interactions"

[22]: Tanabashi et al. (2018), "Review of Particle Physics"

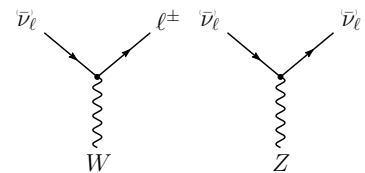


Figure 1.6: Feynman diagrams of charged-current (left) and neutral-current (right) neutrino weak interactions, taken from [23].

Plot is missing + for W and 0 for Z boson.

[20]: Thomson (2013), *Modern particle physics*

[22]: Tanabashi et al. (2018), "Review of Particle Physics"

Neutrino-Lepton Scattering

Neutrino Interactions with Nuclei

To describe the neutrino detection principle of IceCube explained in Chapter 2 we need to understand the weak interaction processes that occur at the energies relevant for this work 10 GeV-100 GeV. The cross-sections are dominated by the following neutrino-nucleon interactions: quasi-elastic scattering (QE), resonant scattering (RES), and deep inelastic scattering (DIS). The relative importance of the different processes depends on energy as can be seen in Figure 1.7.

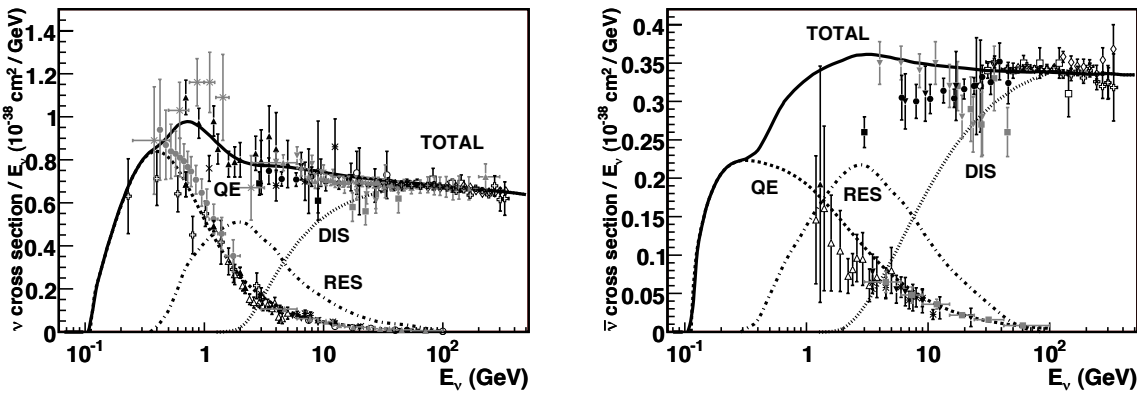


Figure 1.7: Total neutrino(left) and antineutrino(right) per nucleon cross-section divided by neutrino energy plotted against energy. The three main scattering processes quasi-elastic scattering (QE), resonant scattering (RES), and deep-inelastic scattering (DIS) are depicted. Taken from [24].

At energies below 5 GeV, QE and RES occur and the neutrinos interact with approximately point-like protons and neutrons. The cross-sections of these processes are not linear in energy and the transition region to higher energies is poorly understood. At higher energies, the interactions are dominated solely by DIS which has a linear dependence on energy above ~ 20 GeV. For a given neutrino energy, it is possible to predict the cross-section in this region. Here neutrinos interact with a single quark, breaking apart the nucleus and producing a shower of relativistic secondary particles. Neutrino DIS is the primary detection channel of IceCube. From Figure 1.7 it can be seen that the interaction cross-sections are very small of the order of 10^{-38} cm^2 . Because of the small interaction cross-section, very large volume detectors are required to capture a sufficiently large sample of neutrinos to use for precision studies of their properties. For example, the interaction length of a neutrino with $E_\nu = 10 \text{ GeV}$ is of $\mathcal{O}(10^{10} \text{ km})$.

SB: It seems that you have some double counting of information here . I suggest to move some of the information in this "intro" paragraph to the appropriate subsections

Quasi-elastic scattering (QE) with nucleons is the main process below 1 GeV. Protons are converted to neutrons in antineutrino interactions and vice-versa for neutrino interactions. Additionally, a charged lepton corresponding to the neutrino/antineutrino flavor is produced.

Resonant scattering (RES) describes the process of a neutrino scattering off a nucleon producing an excited state of the nucleon in addition to a charged lepton. RES is the leading process at $1.5 \times 10^{-5} \text{ GeV}$ for neutrinos and $1.5 \times 10^{-8} \text{ GeV}$ for antineutrinos.

Deep inelastic scattering (DIS) occurs if a neutrino carries sufficient energy to resolve the underlying structure of the nucleon and interacts with one of the composing quarks. DIS is the dominant process above 10 GeV. The nucleon breaks up and a lepton accompanied by a set of hadronic final states is produced. Whether the lepton is the charged lepton corresponding to the interacting neutrino type, or the neutrino itself depends on the type of DIS interaction. DIS happens via CC as in

$$\begin{aligned} \nu_l + N &\rightarrow l^- + X, \\ \bar{\nu}_l + N &\rightarrow l^+ + X, \end{aligned} \quad (1.23)$$

or NC interactions as

$$\nu_l + N \rightarrow \nu_l + X. \quad (1.24)$$

Here, X stands for any set of final state hadrons and N for the nucleon. The Feynman diagrams for the processes in Equation 1.23 and Equation 1.24 are shown in Figure 1.8.

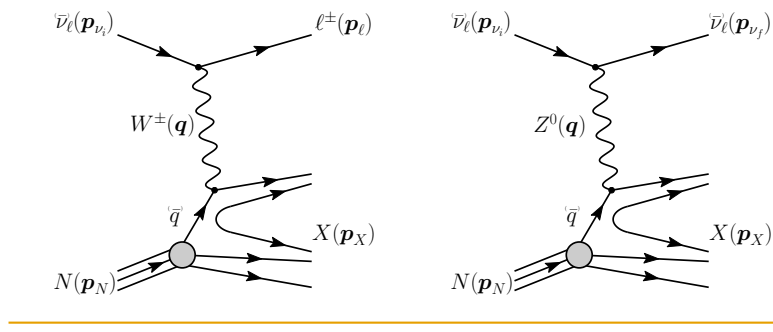


Figure 1.8: Feynman diagrams for deep inelastic scattering of a neutrino with a nucleon via charged-current (left) and neutral current (right) interactions. Taken from [23].

Explain momenta and momentum transfer (p, q) in these figures.

(Re-)write BSM chapter for PhD thesis (just copy paste from M.Sc.).

[22]: Tanabashi et al. (2018), “Review of Particle Physics”

1.4.1 Oscillations

The flux of neutrinos used for this work exclusively comes from the Earth’s atmosphere. When highly relativistic cosmic rays (protons and heavier nuclei [22]) interact in the upper atmosphere they produce a shower of particles. Neutrinos emerge from the decays of charged pions and kaons (π and K mesons) present in these showers. For energies below 100 GeV, the leading contribution comes from the pion decay chain

$$\begin{aligned} \pi^\pm &\rightarrow \mu^\pm + \nu_\mu (\bar{\nu}_\mu), \\ \mu^\pm &\rightarrow e^\pm + \bar{\nu}_\mu (\nu_\mu) + \nu_e (\bar{\nu}_e). \end{aligned} \quad (1.25)$$

The muons that also originate from this process are considered the main background source for IceCube. The left part of Figure 1.9 shows the atmospheric neutrino flux for the very broad energy spectrum in which they are produced. The flux expectations are calculated in the energy range of 100 MeV to 10 TeV for the South Pole [25], where the IceCube detector is located. From Equation 1.25 the ratio between muon and electron neutrinos can be inferred to be $N_{\nu_\mu} : N_{\nu_e} \approx 2 : 1$. This is only the case at muon energies below 1 GeV, where all muons decay in flight. For higher energies, muons can reach earth before decaying increasing the ratio to approximately 10:1 at around 100 GeV as shown in the right part of Figure 1.9. Additionally, kaon decays start to contribute which also increases the number of muons and muon neutrinos.

[25]: Honda et al. (2015), “Atmospheric neutrino flux calculation using the NRLMSISE-00 atmospheric model”

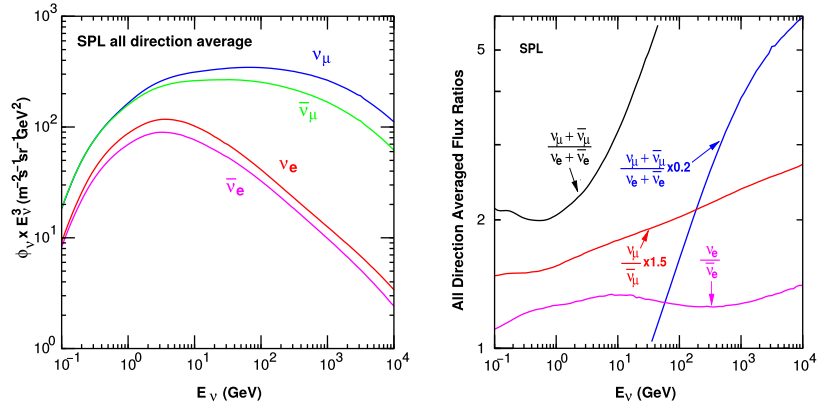


Figure 1.9: Atmospheric neutrino fluxes of the different flavors as a function of energy (left) and ratios between muon- and electron-neutrinos as well as ratios between neutrinos and antineutrinos for both flavors (right). Calculations are done for the geographic South Pole. Taken from [25].

[26]: Fedynitch et al. (2015), "Calculation of conventional and prompt lepton fluxes at very high energy"

SB: You could say why with an extra half-sentence.

[27]: Honda et al. (2007), "Calculation of atmospheric neutrino flux using the interaction model calibrated with atmospheric muon data"

SB: I don't think this is true - the normalization is known to 5% if you trust Anatoli/Juan Pablo. Please have a look at more recent publications on this topic.

[28]: Bilenky et al. (1978), "Lepton mixing and neutrino oscillations"

[22]: Tanabashi et al. (2018), "Review of Particle Physics"

[22]: Tanabashi et al. (2018), "Review of Particle Physics"

SB: formatting/margins also I don't think you defined rho1,2

In cosmic ray interactions, charged mesons or tau particles can also be produced, which leads to the formation of tau neutrinos. However, at the energy range considered for this work, the resulting tau neutrino flux is negligible as compared to the muon neutrino flux [26] and is not taken into account. It should be stated here that there is a rather large uncertainty on the normalization of the atmospheric neutrino flux on the order of 20-30 % [27] in the energy region of interest. This is mainly due to uncertainties in the primary cosmic ray spectrum and modeling of the hadronic interactions.

There are two ways to describe neutrino wave functions based on their Hamiltonian eigenvalues [28], as mass eigenstates or as flavor eigenstates. When applying a plane wave approach to explain the propagation of neutrinos in vacuum, their mass eigenstates evolve as

$$|\nu_k(t)\rangle = e^{-iE_k t/\hbar} |\nu_k\rangle, \quad (1.26)$$

where $E_k = \sqrt{\vec{p}^2 c^2 + m_k^2 c^4}$ is the energy of the mass eigenstate $|\nu_k\rangle$, with momentum \vec{p} and mass m_k . Alternatively, they can be described in terms of their flavor eigenstates, which relate the neutrinos to the charged leptons they interact with in weak CC interactions. The flavor eigenstates are ν_e , ν_μ , and ν_τ , whereas the mass eigenstates are called ν_1 , ν_2 , and ν_3 in the standard three-neutrino model. To understand the propagation of distinct neutrino flavors in time we need to relate the flavor eigenstates to the mass eigenstates. For massive neutrinos, each flavor eigenstate is a superposition of mass eigenstates [22]

$$|\nu_\alpha\rangle = \sum_k U_{\alpha k}^* |\nu_k\rangle, \quad (1.27)$$

where $|\nu_\alpha\rangle$ are the weak flavor states with $\alpha = e, \mu, \tau$ and $|\nu_k\rangle$ the mass states with $k = 1, 2, 3$. $U_{\alpha k}$ is the Pontecorvo-Maki-Nakagawa-Sakata (PMNS) matrix defining the mixing between mass and flavor eigenstates. The mixing matrix can be parameterized as [22]

$$U = \begin{pmatrix} 1 & 0 & 0 \\ 0 & c_{23} & s_{23} \\ 0 & -s_{23} & c_{23} \end{pmatrix} \begin{pmatrix} c_{13} & 0 & s_{13} e^{-i\delta_{CP}} \\ 0 & 1 & 0 \\ -s_{13} e^{i\delta_{CP}} & 0 & c_{13} \end{pmatrix} \begin{pmatrix} c_{12} & s_{12} & 0 \\ -s_{12} & c_{12} & 0 \\ 0 & 0 & 1 \end{pmatrix} \text{diag}(e^{i\rho_1}, e^{i\rho_2}, 1), \quad (1.28)$$

where $c_{ij} = \cos \theta_{ij}$ and $s_{ij} = \sin \theta_{ij}$ are cosine and sine of the mixing angle θ_{ij} , that defines the strength of the mixing between the mass

eigenstates i and j and δ_{CP} is the neutrino CP-violating phase. Nonzero, non-equal neutrino masses and the neutrino mixing relation in Equation 1.27 lead to the observed phenomenon of neutrino oscillations. Oscillation means that a neutrino changes from its initial flavor to another flavor and back after traveling a certain distance. A produced flavor eigenstate $|\nu_\alpha\rangle$ propagates through space as a superposition of mass eigenstates. To find the probability that the initial flavor state $|\nu_\alpha\rangle$ ends up as the final flavor state $|\nu_\beta\rangle$ after the time t we calculate

$$P_{\nu_\alpha \rightarrow \nu_\beta}(t) = |\langle \nu_\beta | \nu_\alpha(t) | \nu_\beta | \nu_\alpha(t) \rangle|^2, \quad (1.29)$$

where P is the probability calculated by applying Fermi's Golden Rule [29]. Fermi's Golden Rule explains the transition rate from one energy eigenstate to another depending on the strength of the coupling between the two. The strength of the coupling is described by the square of the matrix element. Using the unitarity of the mixing matrix $U^{-1} = U^\dagger$ to reverse the relation Equation 1.27 and then time evolve the mass eigenstates with Equation 1.26 we get the time evolution of the flavor state $|\nu_\alpha(t)\rangle$. Inserting this result into Equation 1.29 yields

$$P_{\nu_\alpha \rightarrow \nu_\beta}(t) = \sum_{j,k} U_{\beta j}^* U_{\alpha j} U_{\beta k} U_{\alpha k}^* e^{-i(E_k - E_j)t/\hbar}, \quad (1.30)$$

where the indices j and k run over the mass eigenstates. For small neutrino masses compared to their kinetic energy, we can approximate the energy as

$$E_k \approx E + \frac{c^4 m_k^2}{2E} \quad \rightarrow \quad E_k - E_j \approx \frac{c^4 \Delta m_{kj}^2}{2E}, \quad (1.31)$$

where $\Delta m_{kj}^2 = m_k^2 - m_j^2$ is the mass-squared splitting between states k and j . If we now replace the time in Equation 1.30 by the distance traveled by the relativistic neutrinos $t \approx L/c$ we get

$$\begin{aligned} P_{\nu_\alpha \rightarrow \nu_\beta}(t) &= \delta_{\alpha\beta} - 4 \sum_{j>k} \operatorname{Re}(U_{\beta j}^* U_{\alpha j} U_{\beta k} U_{\alpha k}^*) \sin^2 \left(\frac{c^3 \Delta m_{kj}^2}{4E\hbar} L \right) \\ &\quad + 2 \sum_{j>k} \operatorname{Im}(U_{\beta j}^* U_{\alpha j} U_{\beta k} U_{\alpha k}^*) \sin^2 \left(\frac{c^3 \Delta m_{kj}^2}{4E\hbar} L \right), \end{aligned} \quad (1.32)$$

which is referred to as the survival probability if $\alpha = \beta$ and the transition probability if $\alpha \neq \beta$. The probability in Equation 1.32 is only nonzero if there are neutrino mass eigenstates with masses greater than zero. Additionally, there must be a mass-squared difference Δm^2 and nonzero mixing between the states. Since we assumed propagation in vacuum in Equation 1.26, the transition and survival probabilities correspond to vacuum mixing.

[29]: Dirac (1927), "The Quantum Theory of the Emission and Absorption of Radiation"

1.4.2 Heavy Neutral Lepton Production and Decay in IceCube DeepCore

The IceCube Neutrino Observatory

2

The IceCube Neutrino Observatory [30] is a cubic-kilometer, ice-Cherenkov detector located at the geographic South Pole. IceCube utilizes the Antarctic glacial ice as detector medium to observe neutrinos by measuring the Cherenkov light produced from secondary charged particles. It was deployed between 2006 and 2011 and has been taking data since the installation of the first modules. The primary goal of IceCube is the observation of astrophysical neutrinos as a telescope, but it can also be used to study fundamental particle physics properties by measuring atmospheric neutrinos as well as studying cosmic rays.

This chapter first describes the main- and sub-array of the detector and its detection module in Section 2.1, the propagation of particles through ice is explained in Section 2.2, and finally, the signatures that IceCube can observe of the different particles are introduced in Section 2.3.

add fancy icecube picture
2.1 Detector Components 15
2.2 Particle Propagation in Ice 18
2.3 Event Morphologies 21

[30]: Aartsen et al. (2017), “The IceCube Neutrino Observatory: instrumentation and online systems”

2.1 Detector Components

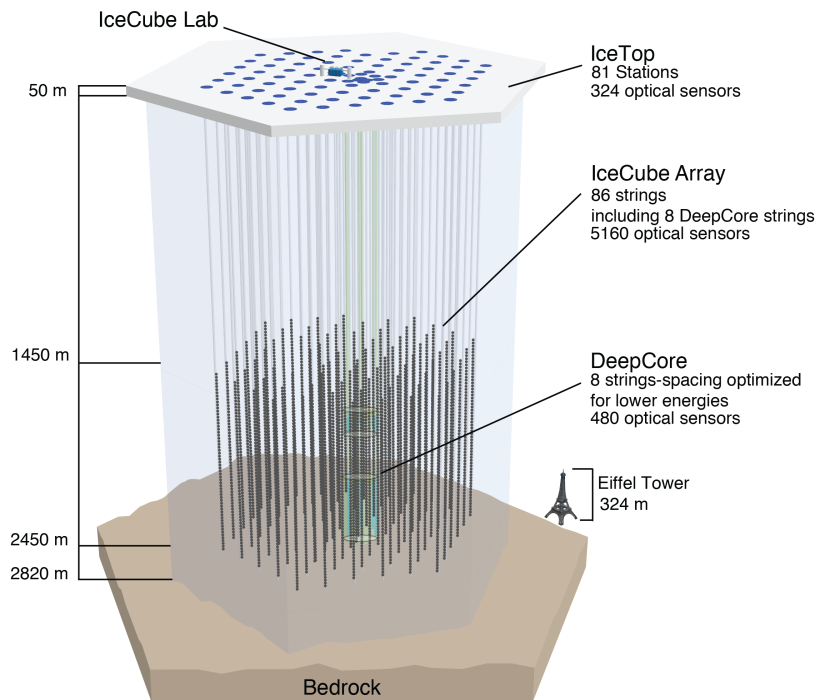


Figure 2.1: Overview of the IceCube detector showing the in-ice main- and sub-array IceCube and DeepCore, IceTop, and the IceCube Laboratory. From [30].

The full IceCube detector array consists of 86 vertical, in-ice strings and 81 surface stations as shown in Figure 2.1. The in-ice part is composed of 60 optical modules per string deployed at depths of 1450 m–2450 m below the ice, while the surface stations of the cosmic air-shower array, *IceTop*, are ice-filled tanks. The surface stations and the majority of the strings are arranged in a hexagonal grid with the operations building, the *IceCube Laboratory* (ICL), central to the grid on the surface. A top view

of the hexagonal arrangement is shown in Figure 2.4. The in-ice array is designed to detect neutrinos in the energy range from GeV to PeV.

2.1.1 Digital Optical Modules and the Antarctic Ice

[31]: Price et al. (2000), "Age vs depth of glacial ice at South Pole"

SB: there are more properties than just these. Somehow need a half sentence that explains why these are particularly important to single out (see ice papers for inspiration)

CL: maybe define that absorption and scattering lengths are? they are defined differently so this invites a comparison that is not so obvious

[32]: Abbasi et al. (2022), "In-situ estimation of ice crystal properties at the South Pole using LED calibration data from the IceCube Neutrino Observatory"

Add reference for the dust layer!

Figure 2.2: Side view of IceCube and DeepCore showing the depth dependent scattering and absorption length (left panel) and the DOM positions around the dust layer.

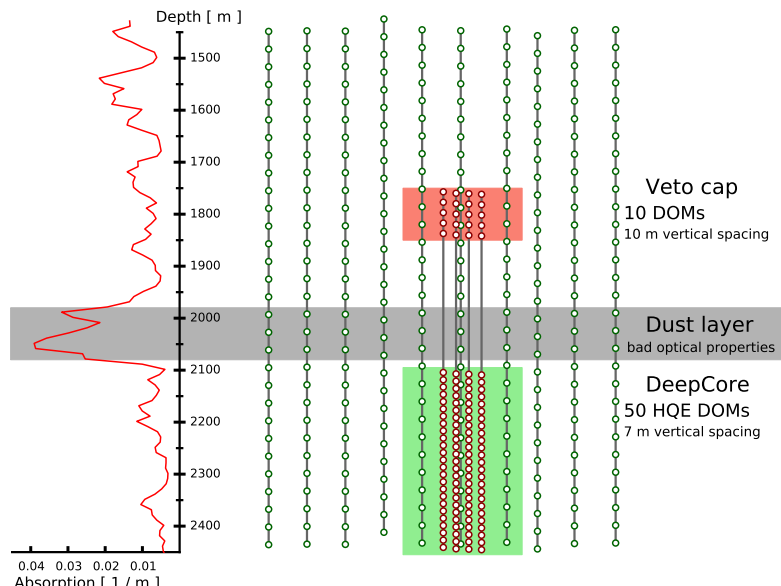
exchange for figure with scattering (check abs/sca is correct)

mention/cite dust logger paper/procedure?

[33]: Abbasi et al. (2009), "The IceCube data acquisition system: Signal capture, digitization, and timestamping"

[33]: Abbasi et al. (2009), "The IceCube data acquisition system: Signal capture, digitization, and timestamping"

The IceCube detection medium is the Antarctic glacial ice itself, which was formed over 100 000 years by accumulation of snow that was subsequently compressed by its own weight to form a dense crystal structure [31]. As a result of this formation process, the optical properties, scattering and absorption, primarily change with depth. Within the detector volume the absorption length ranges from 100 m-400 m, while the scattering length lies between 20 m and 100 m. They are correlated, with the absorption length being roughly four times the scattering length [32]. The vertical distribution of scattering and absorption length can be seen in Figure 2.2, where one dominant feature is the *dust layer* between 2000 m and 2100 m depth. This region has a higher concentration of dust particles that were deposited in a period of high volcanic activity, which leads to bad optical properties in form of larger scattering and absorption.



The ice is instrumented by 5160 optical sensors called *Digital Optical Modules* (DOMs) [33], which can detect the Cherenkov light produced by charged particles traveling through the ice. Each DOM is made of a spherical glass housing, containing a downward-facing Photomultiplier Tube (PMT), the main-board with control, readout, and processing-electronics, and a LED flasher-board for calibration purposes. The design and the individual components of a DOM can be seen in Figure 2.3.

The majority of PMTs are the 10" Hamamatsu R7081-02, which have a bialkali photocathode and are sensitive to wavelengths in the range of 300 nm to 650 nm, with a peak quantum efficiency of 25% at 390 nm. In the central part of the IceCube array the peak efficiency reaches 34%. The dark count rate in the temperature range of -40 °C to -20 °C is ~300 Hz. The DOM electronics measure the PMT voltage and control the gain. At a voltage crossing of the equivalent to 0.25 PE the waveform readout is activated [33]. Only when either one of the nearest or next to nearest

DOMs above or below also sees a voltage crossing within a 1 μ s time window¹, the voltages are digitized and sent to the ICL. Through the application of a waveform unfolding algorithm, called *WaveDeform* [34], the waveforms are compressed, and the results are the reconstructed times and charges of the photo-electrons. This is the basis for all further IceCube data processing.

The PMT is covered with a mu-metal grid (made from wire mesh), shielding the photocathode from Earth's magnetic field, and it is optically coupled to the glass sphere by RTV silicone gel. The glass sphere is a pressure vessel, designed to withstand both the constant ice pressure and the temporary pressure during the refreezing process of the water in the drill hole during deployment (peaking at around 690 bar). The sphere is held by a harness that connects the DOMs along a string and also guides the cable beside them.

The flasher-board controls 12 LEDs that produce optical pulses with a wavelength of 405 nm [30]. The LEDs can be pulsed separately or in combination with variable output levels and pulse lengths. Using the known information of the light source positions and times this can be used for in-situ calibration of the detector by measuring absorption and scattering properties of the ice. Calibrating the absolute efficiency of the DOMs itself is more accurately done using minimum ionizing muons [35, 36], since the total amplitude of the LED light is not well known.

2.1.2 IceCube

The 78 strings that are arranged in a hexagonal pattern from the main part of the in-ice array, which is called *IceCube*. With a ~125 m horizontal spacing between the strings and a ~17 m vertical spacing between DOMs, IceCube has a lower energy threshold of around 100 GeV. IceCube was designed to detect astrophysical neutrinos with energies above 1 TeV.

The coordinate system that is used in IceCube is centered at 46500'E, 52200'N at an elevation of 883.9 m [30]. Per definition, it's a right-handed coordinate system where the y-axis points along the Prime Meridian (Grid North) towards Greenwich, UK, and the x-axis points 90° clockwise from the y-axis (Grid East). The z-axis is normal to the ice surface, pointing upwards. For IceCube analyses depth is defined as the distance along the z axis from the ice surface, assumed to be at an elevation of 2832 m.

2.1.3 DeepCore

The additional 8 strings form a denser sub-array of IceCube called *DeepCore* [37]. It's located at the bottom-center of the in-ice array and its *fiducial volume* also includes the 7 surrounding IceCube strings as shown in Figure 2.4. The strings in this region have a closer average horizontal distance of about 70 m. The lower 50 DeepCore DOMs on each string are placed in the region of clear ice below the dust layer between 2100 m to 2450 m depth, where their vertical spacing is ~7 m. The remaining 10 modules on each string are placed above the dust layer to be used as veto against atmospheric muons as can be seen in Figure 2.2. Additionally, the

1: This is referred to as a *hard local coincidence* (HLC) [33].

[34]: Aartsen et al. (2014), "Energy Reconstruction Methods in the IceCube Neutrino Telescope"

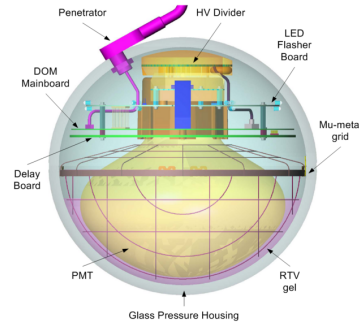


Figure 2.3: Design and components of a Digital Optical Module (DOM) [33]

[30]: Aartsen et al. (2017), "The IceCube Neutrino Observatory: instrumentation and online systems"

[35]: Feintzeig (2014), "Searches for Point-like Sources of Astrophysical Neutrinos with the IceCube Neutrino Observatory"

[36]: Kulacz (2019), "In Situ Measurement of the IceCube DOM Efficiency Factor Using Atmospheric Minimum Ionizing Muons"

Add accuracy of the efficiency calibration here.

[30]: Aartsen et al. (2017), "The IceCube Neutrino Observatory: instrumentation and online systems"

Maybe throw the coordinate system in a box on the side?

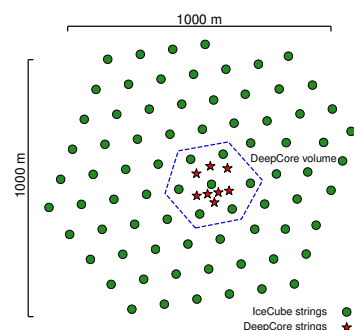


Figure 2.4: Top view of the IceCube array.

Blow up this image a bit, so it's better readable as marginfigure.

[37]: Abbasi et al. (2012), "The design and performance of IceCube DeepCore"

CL: value?

SB: this needs revision. the energy range you mention is particular for oscillations already (atmopsheric neutrinos are plentiful outside of this range you mentioned). If you rewrite the first part you'll have to revisit the second part. Also in general I'd suggest not to rank analyses like Main and Other - DeepCore was orginally intended as a dark matter detector, and there are probably more DM analyses unblinded / year than oscillations. Just keep it general, no need to rank.

[38]: Cherenkov (1937), "Visible Radiation Produced by Electrons Moving in a Medium with Velocities Exceeding that of Light"

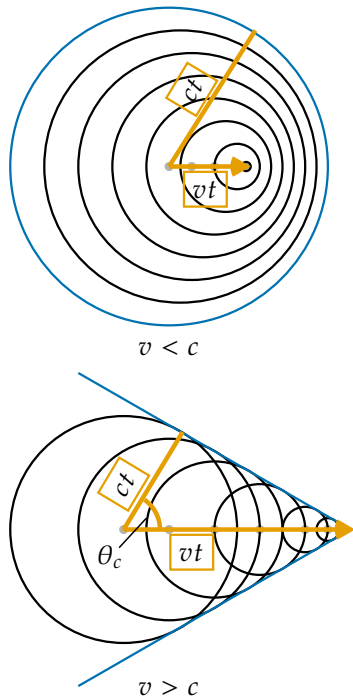


Figure 2.5: Schematic depiction of the spherical light front produced by a particle traveling slower than the speed of light in the medium (top) and the formation of the Cherenkov light front produced by a charged particle traveling faster than the speed of light in the medium (bottom). Blue is the resulting wavefront, while the black circles are spherically emitted light at each position and the orange arrows show the direction of the particle.

DeepCore DOMs are equipped with higher quantum efficiency PMTs. The combination of the denser spacing, the high quantum efficiency modules, and the most favorable ice properties below the dust layer leads to a lower energy detection threshold of around 5 GeV, allowing the more efficient observation of atmospheric neutrinos, which are mostly in the energy range of 10 GeV-100 GeV. The main analysis performed with DeepCore is an atmospheric neutrino oscillation measurement, but the large flux of atmospheric neutrinos allows for many other Beyond Standard Model searches, such as searches for dark matter, non-standard interactions, or sterile neutrinos.

2.2 Particle Propagation in Ice

Neutrinos interacting in the ice via DIS produce muons, electromagnetic showers, and hadronic showers, depending on their flavor and the interaction type. The particles produced in those processes mainly lose their energy through *ionization*, *bremsstrahlung*, *pair production*, and the *photo-nuclear interaction*. Electrically charged particles also emit Cherenkov light when traveling through the ice, which is the main observable in IceCube, but only contributes a small amount to the total energy loss. The Cherenkov effect and the energy losses of the particles are described in the following sections, followed by an overview of the different particle signatures in IceCube.

2.2.1 Cherenkov Effect

When a charged particle moves through a medium with a velocity that is greater than the speed of light in that medium, it emits Cherenkov radiation, losing a very small amount of energy ($\mathcal{O}(10^{-4})$ of the total energy loss). The detection principle of IceCube DeepCore, is based on the observation of resulting Cherenkov photons that are emitted by the charged secondary particles produced in the neutrino interactions that were introduced in Section ???. The Cherenkov effect was first observed by Pavel Cherenkov in 1934 [38] and occurs when the charged particle travels faster than the phase velocity of light, therefore polarizing the medium. Upon de-excitation the molecules emit the received energy as photons in a spherical wavefront. Since the particle moves past this wavefront, the superposition of the spherical light emissions forms a cone, which is shown in blue in the bottom panel of Figure 2.5.

Using trigonometry, the angle θ_c at which the Cherenkov light is emitted can be calculated as

$$\theta_c = \arccos\left(\frac{1}{\beta n}\right), \quad (2.1)$$

where β is the velocity of the particle in units of the speed of light and n is the refractive index of the medium. When the particle velocity is close to the speed of light, the equation holds and the angle is only dependent on the refractive index of the medium. For the Antarctic ice, the refractive index is $n \approx 1.3$ and as a result $\theta_c \approx 41^\circ$.

The frequency of the emission depends on the charge z and the wavelength-dependent index of refraction $n(\omega)$ and is given by the Frank-Tamm

formula [39, 40]

$$\frac{d^2N}{dx d\lambda} = \frac{2\pi\alpha z^2}{\lambda^2} \left(1 - \frac{1}{\beta^2 n(\omega)^2}\right), \quad (2.2)$$

with $\alpha \approx 1/137$ the fine structure constant, λ the wavelength of the emitted light, and x the path length traversed by the particle. Relativistic particles in ice produce roughly 250 photons per cm in the wavelength range of 300 nm-500 nm [41].

2.2.2 Energy Losses

Even though relativistic, charged particles traveling through matter produce Cherenkov radiation, their energy is mainly lost through other processes that are dependent on the particle type and energy. The exact principles of energy loss for the different types can broadly be categorized into the three groups: quasi-continuous energy loss by muons, electromagnetic cascades, and hadronic cascades.

Muons

Muons lose their energy by ionization, bremsstrahlung, pair production, and the photo-nuclear effect. The energy loss by ionization is the dominant process for muons above 1 GeV and has a weak energy dependence given by

$$\left\langle -\frac{dE}{dx} \right\rangle = a_I(E) + b_R(E) \cdot E, \quad (2.3)$$

where E is the energy and $a_I(E)$ and $b_R(E) \cdot E$ are the energy loss by ionization and the combined radiative losses, respectively. In the energy range relevant for this work (10 GeV-100 GeV), the parameters a_I and b_R only depend on energy very weakly and can be approximated by constants. The energy loss is then given by

$$\left\langle -\frac{dE}{dx} \right\rangle = a + b \cdot E. \quad (2.4)$$

Based on this description, there is a critical energy which divides the regimes where ionization and radiative losses dominate. The critical energy is given by $E_{\text{crit}} = a/b$ and for muons in ice it is ~ 713 GeV (using $a \approx 2.59 \text{ MeV cm}^{-1}$ and $b \approx 3.63 \times 10^{-6} \text{ cm}^{-1}$ [42]). Since the energy range of interest is well below this critical energy, the range of a muon can easily be related to its energy by

$$\langle L \rangle = \frac{E_0}{a}. \quad (2.5)$$

Measuring the length of a muon track therefore allows for an estimation of its energy if the full track is contained within the instrumented volume of IceCube. Using the given numbers a 30 GeV muon travels ~ 116 m. This approximate treatment does not take into account the stochastic nature of some energy losses. Bremsstrahlung and photo-nuclear interactions for example rarely occur, but when they do, they deposit a large chunk of energy. A thorough investigation of the energy losses of muons in ice can be found in [43].

Cite n and θ_c

[39]: Frank et al. (1937), "Coherent visible radiation from fast electrons passing through matter"

[40]: Tamm (1991), "Radiation Emitted by Uniformly Moving Electrons"

[41]: Rädel et al. (2012), "Calculation of the Cherenkov light yield from low energetic secondary particles accompanying high-energy muons in ice and water with Geant4 simulations"

SB: you already mentioned that Cher. Rad. doesn't lead to significant energy loss. I suggest to clean up the text a bit, you don't need to emphasize that so many times. Pick one place (probably here) and eliminate it elsewhere

Add reference (PDG or find original)

[42]: Chirkov et al. (2004), "Propagating leptons through matter with Muon Monte Carlo (MMC)"

SB: i like that you give a benchmark value here, for rule of thumb or so, but it should be related to the detector geometry somehow or else it feels too out of place. Give it some context

[43]: Raedel (2012), "Simulation Studies of the Cherenkov Light Yield from Relativistic Particles in High-Energy Neutrino Telescopes with Geant4"

Electromagnetic Showers

Photons as well as electrons and positrons are produced either directly in neutrino interactions or in secondary particle interactions. Above a critical energy E_c , they lose their energy through repeated pair production and bremsstrahlung emission forming an expanding, electromagnetic shower profile. The particles' energy reduces with every interaction and their number increases until they fall below the critical energy where ionization and excitation of surrounding atoms become the dominant energy loss processes for electrons and positrons. For photons the remaining energy is lost through the Compton effect and the photoelectric effect. Below the critical energy no new shower particles are produced. Electromagnetic cascades can be characterized by the radiation length, X_0 , after which electrons/positrons reduced their energy to $1/e$ of their initial energy. For photons, it's equivalent to $7/9$ of the mean free path of pair production. The critical energy for ice is $E_c \approx 78$ MeV, with a radiation length of $X_0 \approx 39.3$ cm [22].

Add reference for these processes.

[22]: Tanabashi et al. (2018), "Review of Particle Physics"

cite em shower distribution

The radiation length governs the longitudinal shower profile and using $t = x/X_0$, the shower intensity can be described by

$$\frac{dE}{dt} = E_0 b \frac{(bt)^{a-1} e^{-bt}}{\Gamma(a)}, \quad (2.6)$$

[43]: Raedel (2012), "Simulation Studies of the Cherenkov Light Yield from Relativistic Particles in High-Energy Neutrino Telescopes with Geant4"

[44]: Agostinelli et al. (2003), "Geant4—a simulation toolkit"

Add angular profile plot (Summer agrees!) (create one based on Leif Rädel as Alex did)

SB: rephrase gamma (from equation) is not defined

where a and b are parameters that have to be estimated from experiment. Based on the work from [43], performed with Geant4 [44], the parameters for electromagnetic showers in ice are

$$e^- : a \approx 2.01 + 1.45 \log_{10}(E_0/\text{GeV}), b \approx 0.63, \quad (2.7a)$$

$$e^+ : a \approx 2.00 + 1.46 \log_{10}(E_0/\text{GeV}), b \approx 0.63, \quad (2.7b)$$

$$\gamma : a \approx 2.84 + 1.34 \log_{10}(E_0/\text{GeV}), b \approx 0.65. \quad (2.7c)$$

The maximum of the shower is at $t_{max} = (a - 1)/b$ and the Cherenkov emission of the charged particles produced in the shower is peaked around the Cherenkov angle, since they are produced in the forward direction.

Hadronic Showers

The breaking nucleus or any hadronic decay products from the neutrino DIS interactions always create a hadronic cascade. It is a result of secondary particles produced in strong interactions between the hadrons and the traversed matter. The charged particles produced in the shower will emit Cherenkov radiation, while neutral particles will be invisible to the detector. There is also an electromagnetic component of the shower, due to for example the decay of neutral pions into photons. Hadronic showers of the same energy as electromagnetic showers have larger fluctuations in energy deposition and shape, since they depend on the produced particle types. Hadrons also have a higher energy threshold for Cherenkov light production, because of their higher mass. Based on [43, 45], the visible electromagnetic fraction of hadronic showers can be

[43]: Raedel (2012), "Simulation Studies of the Cherenkov Light Yield from Relativistic Particles in High-Energy Neutrino Telescopes with Geant4"

[45]: Gabriel et al. (1994), "Energy dependence of hadronic activity"

parameterized as

$$F(E_0) = \frac{T_{\text{hadron}}}{T_{\text{EM}}} = 1 - (1 - f_0) \left(\frac{E_0}{E_s} \right)^{-m}, \quad (2.8)$$

where $T_{\text{hadron/EM}}$ is the total track length of a hadronic/electromagnetic shower with the same energy, f_0 is the ratio of hadronic and electromagnetic light yield, E_0 is the initial energy, and E_s is an energy scale. The parameter m is an arbitrary parameter. The ratio $F(E_0)$ increases with energy, but is always smaller than 1. The variance of this distribution is given by

$$\sigma_F(E_0) = \sigma_0 \log(E_0)^{-\gamma}. \quad (2.9)$$

The parameters m , E_s , and f_0 are fit from simulation. Cherenkov light from hadronic showers also peaks around the Cherenkov angle, but the angular distribution is more smeared out, due to the variations in particle type and their energy depositions.

SB: Explain

2.3 Event Morphologies

The event morphologies produced by particles detected in IceCube are combinations of the three energy loss types described in Section 2.2.2, e.g. *cascades* from electromagnetic and hadronic showers and elongated *tracks* from muons traveling through the detector. Table 2.1 gives an overview of the possible event signatures.

Interaction	Secondary particles	Signature
CC $\nu_\mu^{(-)}$	μ^\pm track	Track-only
	μ^\pm track and hadrons	Cascade + track
CC $\nu_\tau^{(-)}$	τ^\pm decaying into μ^\pm (~17% BR), hadrons	
	τ^\pm decaying into e^\pm or hadrons (~83% BR)	
CC $\nu_e^{(-)}$	e^\pm , hadrons	Cascade-only
NC $\nu_\ell^{(-)}$	hadrons	

Table 2.1: IceCube low energy event signatures, their underlying interaction type, and the particles that produce them. Also shown are the secondary particles produced in the interactions. Black dashed lines represent neutrinos, green lines muons, orange line leptons, and blue and red lines are particles in electromagnetic and hadronic cascades, respectively. Adapted from [23].

Neutrino interactions are observed as cascades, tracks, or a combination of both, depending on the initial flavor and the interaction type for the specific event.

In ν_μ - CC interactions, a muon is produced in addition to a hadronic shower from the breaking nucleus. If the interaction happens outside the detector, but the muon passes through the detector, this will create a track-like signature. The same happens if the interaction happens inside, but the energy transfer to the nucleus is small ($y \approx 0$). At energies relevant for this work, tracks have length at the same order of the distance between DOMs, so they can be observed as such.

Make sure I have this defined in the SM interaction chapter!

If the interaction happens inside the detector and the energy transfer to the hadronic part of the shower is larger, it will create a cascade with a track leaving it. A similar signature is observed after a ν_τ - CC interaction, in which a tau is produced that later decays into a muon, with a branching ratio of 17 %. In those cases the muon usually has a lower energy and the track will be fainter and harder to observe.

The other 83 % of ν_τ - CC interactions produce a tau that decays into an electron or hadrons, leaving a cascade-only signature through the electromagnetic or hadronic shower. All ν_e - CC interactions also produce pure cascades, since the electron quickly loses its energy in an electromagnetic shower. In all ν - NC interactions, the produced neutrino escapes and only the hadronic shower is observable. Since the size of the cascades at the energy range of interest is smaller than the spacing of the DOMs, they are approximately observed as point-like, spherical light sources. Considering the short effective scattering length (20 m-50 m), the light is almost isotropically emitted.

SB: Since your analysis depends on the ability to reconstruct cascade directions, it seems odd to emphasize that the light is nearly isotropically emitted. Of course that is true, but the emphasis should rather be on the fact that there remains some asymmetry to the light profile

Atmospheric muons also produce pure track like signatures, similar to ν_μ - CC interactions happening outside the detector. They are one of the main backgrounds for analyses using atmospheric neutrinos and are therefore the target of many filter steps described in Section ??.

Heavy Neutral Lepton Signal Simulation

3

After the SM simulation generation and the default low energy event selection and processing chain were introduced in the previous Chapter ??, the focus will now be on the central part of this thesis - the HNL signal simulation. Since this is the first search for HNLs with IceCube DeepCore, there was no prior knowledge of the number of events expected per year nor of the expected performance in terms of reconstruction and classification accuracy which governs the 90 % confidence level on estimateing the $|U_{\tau 4}|^2$ mixing matrix element. This is the first simulation developed for IceCube DeepCore. Two avenues of simulation generation were pursued in parallel. The physically accurate, model dependent simulation is described in Section 3.2 and a collection of model independent simulation sets was realized and is explained in Section 3.1. The latter is used for performance benchmarking and as a cross-check for the model dependent simulation

Adapt to reflect switched chapter order	
3.1 Model Independent	
Simulation	23
3.2 Model Dependent Simula-	
tion	27

3.1 Model Independent Simulation

To investigate the potential of IceCube to detect HNLs by identifying the unique double cascade morphology explained in Section 1.4.2, it is very valuable to have simulation sets where the double cascade kinematics can be controlled directly. In a realistic model the decay kinematics and the absolute event expectation all depend on the specific model parameters chosen (see Section ??). To decouple the simulation from a specific parameter choice, a model independent double cascade generator was developed. Using this generator a few simulation sets were produced to investigate the performance of IceCube DeepCore to detect low energetic double cascades, dependent on their properties. The results of this study will be discussed in Chapter ??.

3.1.1 Generator Functions

In order to produce the model independent simulation a series of generator functions was implemented in PYTHON [46]. The collection of functions can be found in [this public repository](#). A few independent functions are needed to perform the sampling based on a random variable between 0 and 1 as input. There is a simple function to return a random sign (+1/-1) and two functions to sample from a power law and an exponential distribution. The inputs are the wanted sampling range and the power law index or the exponential decay constant, respectively. They both apply the inverse transformation method.

[46]: Van Rossum et al. (2009), *Python 3 Reference Manual*

Additionally, there are some functions that are IceCube specific. Two functions are implemented to transform a direction from IceCube zenith/azimuth angles to a direction vector and vice versa. There is a function to create an EM cascade particle from position, direction, energy, and time and another to produce an arbitrary list of EM cascades, with the

previous function, given the list of input parameters, and then adding it to the current IceCube event. Based on these functions, any specific simulation set can be produced by choosing the sampling distributions and number of cascades to be placed in each event and then calling the generator functions with the input parameters based on these sampling distributions.

IceCube software framework

The functions described above are based on the (public) `icetray` software project and the EM particles are defined as type `I3Particle`, while the object to store the MC particles is called `I3MCTree` and each IceCube event information is in one `I3Frame` object.

3.1.2 Simplistic Sets

Make my own DC string positions/distances plot version.

To investigate some idealistic double cascade event scenarios, two sets are produced for straight up-going events that are centered on a string and horizontal events located inside DeepCore.

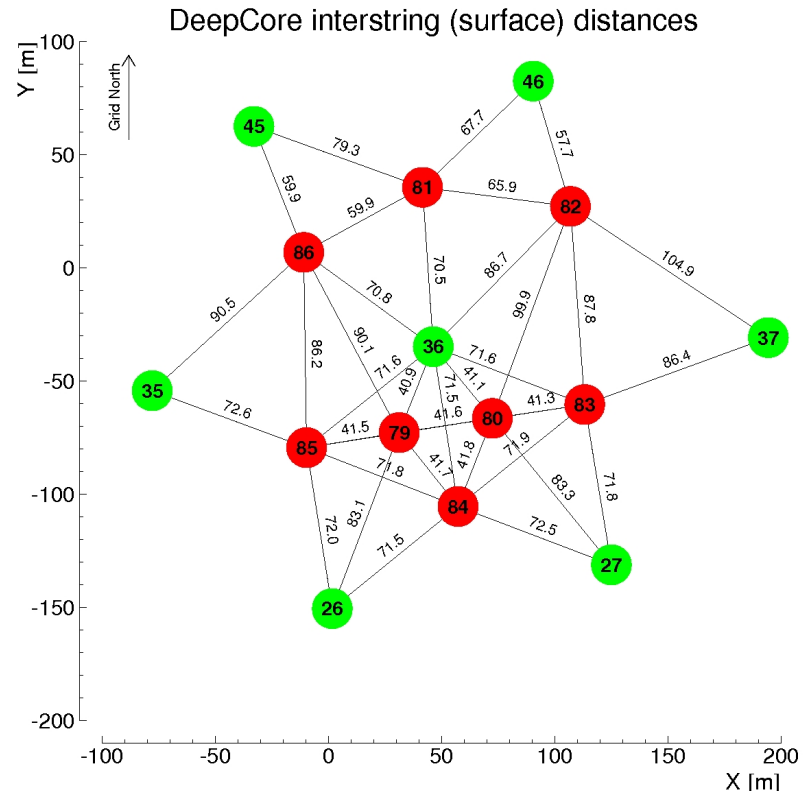


Figure 3.1: Horizontal positions and distances between DeepCore strings. Red strings are instrumented more densely (vertically) and partially have higher quantum efficiency (HQE) DOMs.

The first set is used to investigate one of the most promising scenarios to detect a double cascade, where both cascade centers are located on a DeepCore string (namely string 81) and the directions are directly up-going. The horizontal positions and distances of all DeepCore fiducial volume strings are shown in Figure 3.1 and string 81 is at a medium distance of ~ 70 m to its neighboring strings. As already mentioned in Section 2.1.3, DeepCore strings have higher quantum efficiency DOMs and a denser vertical spacing, making them better to detect low energetic

Set	Variable	Distribution	Range/Value
Up-going			
	energy	uniform	0.0 GeV to 60.0 GeV
	zenith	fixed	180.0°
	azimuth	fixed	0.0°
	x, y position	fixed	(41.6, 35.49) m
	z position	uniform	-480.0 m to -180.0 m
Horizontal			
	energy	uniform	0.0 GeV to 60.0 GeV
	zenith	fixed	90.0°
	azimuth	uniform	0.0° to 360.0°
	x, y position	uniform (circle)	c=(46.29, -34.88) m, r=150.0 m
	z position	fixed	-330.0 m

Table 3.1: Generation level sampling distributions and ranges/values of up-going and horizontal model independent simulation.

events that produce little light. To produce the events, the x, y position of the cascades is fixed to the center of string 81 while the z position is sampled uniformly along the axis of the string. The energies are sampled uniformly between 0.0 GeV and 60.0 GeV. The specific sampling distributions/values for the cascades are listed in Table 3.1. The order of the cascades is chosen such that the lower one is first ($t_0 = 0.0$ ns) and the upper one is second ($t_1 = L/c$), assuming the speed of light c as speed of the heavy mass state, traveling between the two cascades.

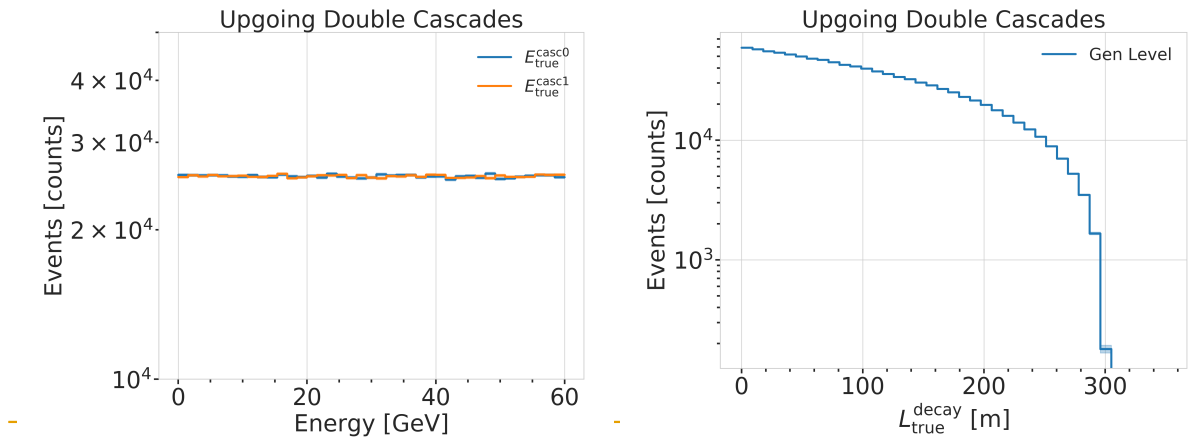


Figure 3.2: Generation level distributions of the simplistic simulation sets. Cascade and total energies (left) and decay lengths (right) of both sets are shown.

Re-make plot with all energies (left) and decay lengths (right) of both sets (they are the same))

Re-make plot with all decay lengths (both sets)

The second set is used to investigate the reconstruction performance for horizontal events, where the spacing between DOMs is much larger. The cascades are placed uniformly on a circle centered in DeepCore. The direction is always horizontal and azimuth is defined by the connecting vector of both cascade positions. The energies are again sampled uniformly between 0.0 GeV and 60.0 GeV and the detailed sampling distributions/values are also listed in Table 3.1. Some examples of the generation level distributions of the simplified sets are shown in Figure 3.2, while further distributions can be found in Figure A.1. The variables that are uniformly sampled or fixed to a certain value are not presented.

Table 3.2: Generation level sampling distributions and ranges/values of the realistic model independent simulation.

Variable	Distribution	Range/Value
energy (total)	power law E^{-2}	1 GeV to 1000 GeV
decay length	exponential $e^{-0.01L}$	0 m to 1000 m
zenith	uniform	70° to 180°
azimuth	uniform	0° to 360°
x, y (one cascade)	uniform (circle)	$c=(46.29, -34.88)$ m, $r=150$ m
z (one cascade)	uniform	-480.0 m to -180.0 m

3.1.3 Realistic Set

To thoroughly investigate the potential of IceCube DeepCore to detect double cascade events, a more realistic simulation set is produced that aims to be as close as possible to the expected signal simulation explained in Section 3.2, while still allowing some freedom to control the double cascade kinematics. For this purpose the total energy is sampled from an E^{-2} power law, mimicking the energy spectrum of the primary neutrinos as stated in Section ???. Although in the realistic process described in Section 3.2 the energy is distributed in a more complex way into the two cascades and secondary particles, it is a good approximation to simply divide the total energy into two parts. This is done by randomly assigning a fraction between 0 % and 100 % to one cascade and the remaining part to the other cascade. In this way the whole sample covers various cases of energy distributions between the two cascades. To efficiently generate events in a way that produces distributions similar to what would be observed with DeepCore, one of the cascade positions is sampled inside the DeepCore volume by choosing its coordinates randomly on a cylinder that is centered in DeepCore. This is similar to a trigger condition of one cascade always being inside the DeepCore fiducial volume. By choosing the direction of the event sampling zenith and azimuth uniformly between 70° and 180° and 0° and 360°, respectively, the position of the other cascade can be inferred for a given decay length. The length is sampled from an exponential distribution, which would be expected for the decaying heavy mass state. Based on the direction and the decay length, the position of the other cascade is found, assuming a travel speed of c and randomly choosing whether the cascade position that was sampled is the first cascade or the second and then assigning the other cascade position accordingly. The sampling distributions/values are listed in Table 3.4. Example distributions of the generation level variables are shown in Figure 3.3, while further distributions can be found in Figure A.2.

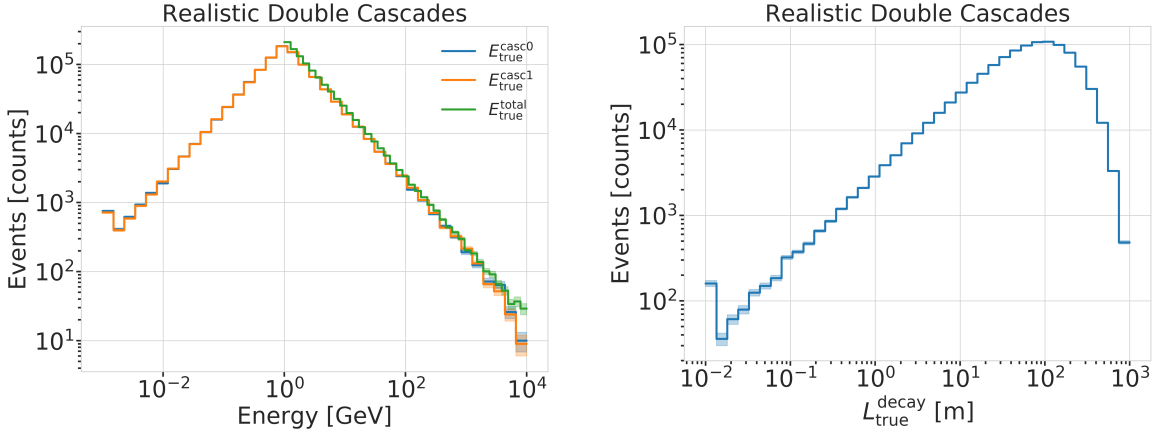


Figure 3.3: Generation level distributions of the simplistic realistic set. Shown are the cascade and total energies (left) and decay lengths (right).

3.2 Model Dependent Simulation

To estimate the HNL event expectation in IceCube DeepCore, depending on the specific model parameters, a generator was developed that is based on the HNL theory introduced in Section ???. For this work, only the interaction with the τ -sector was taken into account ($|U_{\alpha 4}^2| = 0$, $\alpha = e, \mu$), which reduces the physics parameters of interest and relevant for the simulation to the fourth heavy lepton mass, m_4 , and the mixing, $|U_{\tau 4}^2|$. The generator uses a customized *LEPTONINJECTOR* (*LI*) version to create the events and *LEPTONWEIGHTER* (*LW*) to weight them [47]. The modified *LI* and the essential components needed for the HNL simulation are described in the next sections, followed by the description of the weighting scheme and the sampling distributions chosen for the simulation generation.

[47]: Abbasi et al. (2021), “LeptonInjector and LeptonWeighter: A neutrino event generator and weighter for neutrino observatories”

3.2.1 Custom LeptonInjector

In its standard version, the *LI* generator produces neutrino interactions by injecting a lepton and a cascade¹ at the interaction vertex of the neutrino, where the lepton is the charged (neutral) particle produced in a CC (NC) interaction and the cascade is the hadronic cascade from the breaking nucleus. Both objects are injected with the same (x, y, z, t) coordinates and the kinematics are sampled from the differential and total cross-sections that are one of the inputs to *LI*.

1: The cascades are defined as icetray I3Particles with type *Hadrons*.

In the modified version, the SM lepton at the interaction vertex is replaced by the new HNL particle, where the interaction cross-sections are replaced by custom, mass dependent HNL cross-sections. The HNL is forced to decay after a chosen distance to produce secondary SM particles, where the decay mode is randomly chosen based on the mass dependent branching ratios from the kinematically accessible decay modes shown in Figure 3.4. The cross-section and decay width calculations were implemented for this purpose and will be explained in more detail in the following. Another needed addition to *LI* is that the decay products of the HNL are also added to the list of MC particles in each event. They

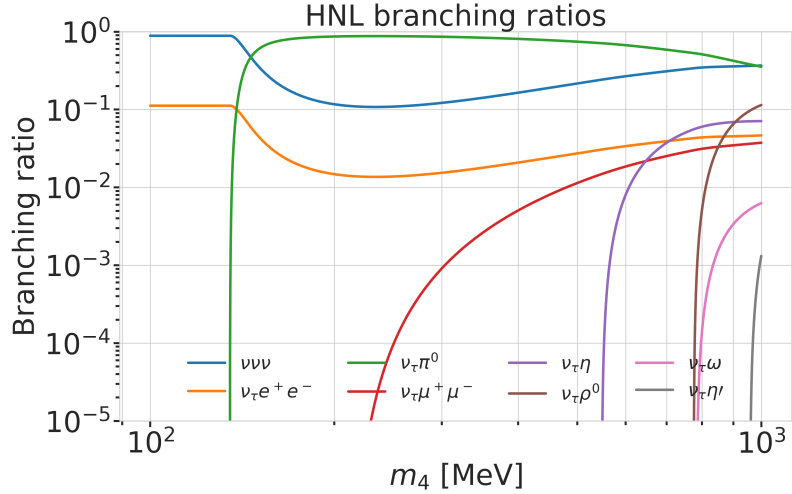


Figure 3.4: Branching ratios of the HNL within the mass range considered in this work, only considering $|U_{\tau 4}^2| \neq 0$, calculated based on the results from [19].

[48]: Alwall et al. (2014), “The automated computation of tree-level and next-to-leading order differential cross sections, and their matching to parton shower simulations”

are injected with the correctly displaced position and delayed time from the interaction vertex, given the HNL decay length. These HNL daughter particles form the second cascade, not as a single hadronic cascade object, but as the explicit particles forming the shower. The kinematics of the two-body decays are computed analytically, while the three-body decay kinematics are calculated with `MADGRAPH` [48], which will also be explained further below. Independent of the number of particles in the final state of the HNL decay, the kinematics are calculated/simulated at rest and then boosted along the HNL momentum.

The injection is done using the *LI volume mode*, for the injection of the primary particle on a cylindrical volume, adding 50 % of the events with ν_τ and the other half with $\bar{\nu}_\tau$ as primary particle types. The generator takes the custom double-differential/total cross-section splines described below and the parameters defining the sampling distributions as inputs.

Cross-Sections

The cross-sections are calculated using the `NuXSSplMkr` [49] software, which is a tool to calculate neutrino cross-sections from *parton distribution functions (PDFs)* and then produce splines that can be read and used with `LI/LW`. The tool was customized to produce the custom HNL cross-sections, where the main modification to calculate the cross-sections for the ν_τ -NC interaction into the new heavy mass state is the addition of a kinematic condition to ensure that there is sufficient energy to produce the heavy mass state. It is the same condition that needs to be fulfilled for the CC case, where the outgoing charged lepton mass is non-zero. Following [50] (equation 7), the condition

$$(1 + x\delta_N)h^2 - (x + \delta_4)h + x\delta_4 \leq 0 \quad (3.1)$$

is implemented for the NC case in the `NuXSSplMkr` code. Here $\delta_4 = \frac{m_4^2}{s-M^2}$, $\delta_N = \frac{M^2}{s-M^2}$, and $h \stackrel{\text{def}}{=} xy + \delta_4$, with x, y being the Bjorken variables, m_4 and M the mass of the heavy state and the target nucleon, respectively, and s the center of mass energy squared.

[50]: Levy (2009), “Cross-section and polarization of neutrino-produced tau’s made simple”

Re-make plot with 3 target masses and better labels

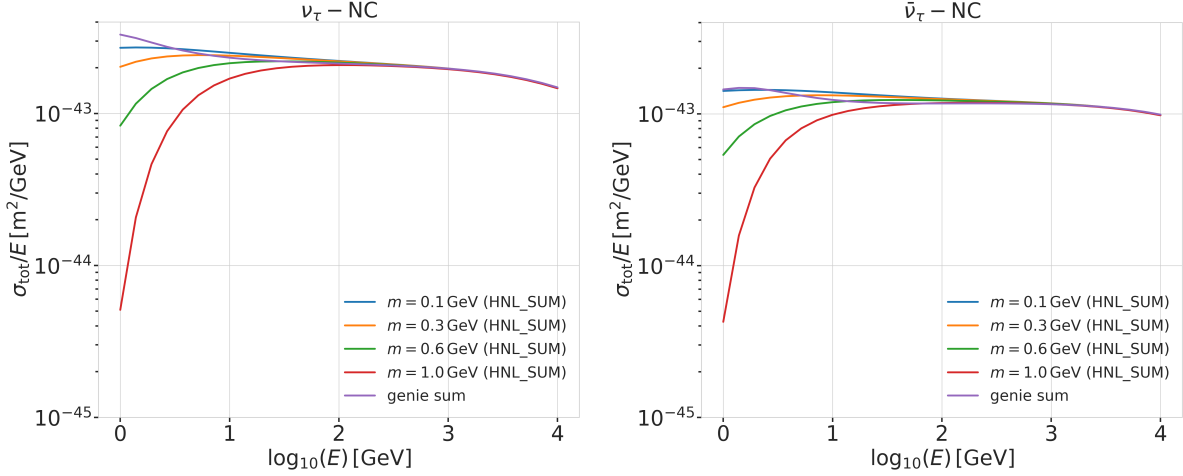


Figure 3.5: Custom HNL total cross-sections for the four target masses compared to the total ($\nu_\tau/\bar{\nu}_\tau$ NC) cross-section used for SM neutrino simulation production with GENIE.

As already described in Section ??, the SM neutrino background simulation is created using the GRV98LO PDFs. These PDFs also had to be added to the cross-section spline maker, to ensure good agreement between the background and signal cross-sections. The double differential ($d\sigma/dx dy$) and total (σ) cross-sections were produced for the chosen target HNL masses and then splined. The produced cross-section are added to the custom LI version and used for the simulation generation and weighting. Figure 3.5 shows the total cross-sections that were produced compared to the cross-section used for the production of the SM $\nu_\tau/\bar{\nu}_\tau$ NC background simulation. Above $\sim 2 \times 10^2$ GeV they match, which is the wanted result of using the identical input PDFs.

Decay Channels

The accessible decay channels are dependent on the mass of the HNL and the allowed mixing. For this analysis, where only $|U_{\tau 4}|^2 \neq 0$, the considered decay channels are listed in Table 3.3 and the corresponding branching ratios are shown in Figure 3.4. The individual branching ratio for a specific mass is calculated as $BR_i(m_4) = \Gamma_i(m_4)/\Gamma_{\text{total}}(m_4)$, where $\Gamma_{\text{total}}(m_4) = \sum \Gamma_i(m_4)$. The formulas to calculate the decay widths show up in multiple references, but we chose to match them to [19], which also discusses the discrepancies in previous literature.

2-Body Decay Widths The decay to a neutral pseudoscalar meson is

$$\Gamma_{\nu_4 \rightarrow \nu_\tau P} = |U_{\tau 4}|^2 \frac{G_F^2 m_4^3}{32\pi} f_P^2 (1 - x_p^2)^2, \quad (3.2)$$

with $x_P = m_P/m_4$ and the *effective decay constants* given by

$$f_{\pi^0} = 0.130 \text{ GeV}, \quad f_\eta = 0.0816 \text{ GeV}, \quad f_{\eta'} = -0.0946 \text{ GeV}, \quad (3.3)$$

Add comparisons of SM cross-sections between NuXSSplMkr and genie?

add varied total cross-section for a few background HNL events (for QE/RES variations?!)

[19]: Coloma et al. (2021), “GeV-scale neutrinos: interactions with mesons and DUNE sensitivity”

Channel	Opens	\hat{BR}
$\nu_4 \rightarrow \nu_\tau \nu_\alpha \bar{\nu}_\alpha$	0 MeV	1.0
$\nu_4 \rightarrow \nu_\tau e^+ e^-$	1 MeV	?
$\nu_4 \rightarrow \nu_\tau \pi^0$	135 MeV	?
$\nu_4 \rightarrow \nu_\tau \mu^+ \mu^-$	211 MeV	?
$\nu_4 \rightarrow \nu_\tau \eta$	548 MeV	?
$\nu_4 \rightarrow \nu_\tau \rho^0$	770 MeV	?
$\nu_4 \rightarrow \nu_\tau \omega$	783 MeV	?
$\nu_4 \rightarrow \nu_\tau \eta'$	958 MeV	?

Table 3.3: Possible decay channels of the HNL, considering only $|U_{\tau 4}|^2 \neq 0$. Listed is the mass at which each channel opens and the maximum branching ratio.

Calculate max BRs

while the decay to a neutral vector meson is given by

$$\Gamma_{\nu_4 \rightarrow \nu_\tau V} = |U_{\tau 4}|^2 \frac{G_F^2 m_4^3}{32\pi} \left(\frac{f_V}{m_V} \right)^2 g_V^2 (1 + 2x_V^2)(1 - x_V^2)^2, \quad (3.4)$$

with $x_V = m_V/m_4$,

$$f_{\rho^0} = 0.171 \text{ GeV}^2, \quad f_\omega = 0.155 \text{ GeV}^2, \quad (3.5)$$

and

$$g_{\rho^0} = 1 - 2 \sin^2 \theta_w, \quad g_\omega = \frac{-2 \sin^2 \theta_w}{3}, \quad \sin^2 \theta_w = 0.2229 \quad (3.6)$$

[51]: Tiesinga et al. (2021), “CODATA recommended values of the fundamental physical constants: 2018”

3-Body Decay Widths The (invisible) decay to three neutrinos is

$$\Gamma_{\nu_4 \rightarrow \nu_\tau \nu_\alpha \bar{\nu}_\alpha} = |U_{\tau 4}|^2 \frac{G_F^2 m_4^5}{192\pi^3}, \quad (3.7)$$

while the decay to two charged leptons (using $x_\alpha = (m_\alpha/m_4)^2$) of the same flavor reads

$$\Gamma_{\nu_4 \rightarrow \nu_\tau l_\alpha^+ l_\alpha^-} = |U_{\tau 4}|^2 \frac{G_F^2 m_4^5}{192\pi^3} [C_1 f_1(x_\alpha) + C_2 f_2(x_\alpha)], \quad (3.8)$$

with the constants defined as

$$C_1 = \frac{1}{4}(1 - 4s_w^2 + 8s_w^4), \quad C_2 = \frac{1}{2}(-s_w^2 + 2s_w^4), \quad (3.9)$$

the functions as

$$f_1(x_\alpha) = (1 - 14x_\alpha - 2x_\alpha^2 - 12x_\alpha^3)\sqrt{1 - 4x_\alpha} + 12x_\alpha^2(x_\alpha^2 - 1)L(x_\alpha), \quad (3.10)$$

$$f_2(x_\alpha) = 4[x_\alpha(2 + 10x_\alpha - 12x_\alpha^2)\sqrt{1 - 4x_\alpha} + 6x_\alpha^2(1 - 2x_\alpha + 2x_\alpha^2)L(x_\alpha)], \quad (3.11)$$

and

$$L(x) = \ln \left(\frac{1 - 3x - (1 - x)\sqrt{1 - 4x}}{x(1 + \sqrt{1 - 4x})} \right). \quad (3.12)$$

JVS: consider also writing down the (trivial) 2-body decay kinematics for completeness and consistency.
This transition is a bit jarring as it is

[19]: Coloma et al. (2021), “GeV-scale neutrinos: interactions with mesons and DUNE sensitivity”

3-Body Decay Kinematics with MadGraph

The specific MadGraph version used to produce the 3-body decay kinematics is [MadGraph4 v3.4.0](#). As input, the decay diagrams calculated with [FeynRules 2.0](#) using the Lagrangians derived in [19]. The Universal FeynRules Output (UFO) from [EFFECTIVE_HEAVYN_MAJORANA_v103](#) were used for our calculation. For each mass and corresponding decay channels, we produce 1×10^6 decay kinematic variations in the rest frame and store those in a text file. During event generation, we uniformly select an event from that list, to simulate the decay kinematics of a 3-body decay.

3.2.2 Sampling Distributions

In principle, the generation level sampling distributions should be chosen such that at final level of the selection chain the phase space relevant for the analysis is covered with sufficient statistics to make a reasonable estimate of the event expectation. Insufficiently large initial distributions lead to an underestimate of the expected rates, because part of the events that would pass the selection are not produced. This would still be correct as in being the more conservative estimate, but it would limit the analysis potential. Three discrete simulation sets were produced with HNL masses of 0.3 GeV, 0.6 GeV and 1.0 GeV. Each set consists of a part that is generated for very short decay lengths and one for long decay lengths, because during development it became clear that the low lengths component is crucial to get a reasonable event estimate. The remaining sampling distributions are identical for all sets and are listed in Table 3.4. The target number of events for each set was 2.5×10^9

Variable	Distribution	Range/Value
energy	E^{-2}	[2 GeV, 1×10^4 GeV]
zenith	uniform (in $\cos(\theta)$)	[80°, 180°]
azimuth	uniform	[0°, 360°]
vertex x, y	uniform	$r=600$ m
vertex z	uniform	-600 m to 0 m
m_4	fixed	[0.3, 0.6, 1.0] GeV
L_{decay}	L^{-1}	[0.0004, 1] m / [1, 1000] m

Table 3.4: Generation level sampling distributions and ranges/values of the model dependent simulation sets.

3.2.3 Weighting Scheme

To produce physically correct event distributions based on the arbitrary generation sampling distributions for the HNL simulation, the forward folding method that was already introduced for the SM simulation in Section ?? is used again. How this will be applied in the analysis is discussed in Section ???. The weighting scheme that will be explained in the following is implemented in the IceCube low energy analysis framework PISA, which will be discussed in Section ???. The custom weighting scheme is implemented in [this custom stage](#). The only needed input is the mixing strength $|U_{\tau 4}|^2$, which is the variable physics parameter in this analysis. This weighting is needed to go from the used decay length sampling distribution (inverse $1/L$ with fixed range in lab frame) to the target distribution (exponential defined by proper lifetime of the HNL). For each event the additional weight is calculated using the gamma factor

$$\gamma = \frac{\sqrt{E_{\text{kin}}^2 + m_4^2}}{m_4}, \quad (3.13)$$

with the HNL mass m_4 and its kinetic energy E_{kin} . The speed of the HNL is calculated as

$$v = c \cdot \sqrt{1 - \frac{1}{\gamma^2}}, \quad (3.14)$$

where c is the speed of light. With these the lab frame decay length range $[s_{\min}, s_{\max}]$ can be converted into the rest frame lifetime range $[\tau_{\min}, \tau_{\max}]$

for each event

$$\tau_{\min/\max} = \frac{s_{\min/\max}}{v \cdot \gamma}. \quad (3.15)$$

The proper lifetime of each HNL event can be calculated using the total decay width Γ_{total} from Section 1 and the chosen mixing strength $|U_{\tau 4}|^2$ as

$$\tau_{\text{proper}} = \frac{\hbar}{\Gamma_{\text{total}}(m_4) \cdot |U_{\tau 4}|^2}, \quad (3.16)$$

where \hbar is the reduced Planck constant. Since the decay lengths or lifetimes of the events are sampled from an inverse distribution instead of an exponential, as it would be expected from a particle decay, we have to re-weight accordingly to achieve the correct decay lengths or lifetimes distribution. This is done by using the wanted exponential distribution

$$\text{PDF}_{\text{exp}} = \frac{1}{\tau_{\text{proper}}} \cdot e^{\frac{-\tau}{\tau_{\text{proper}}}}, \quad (3.17)$$

and the inverse distribution that was sampled from

$$\text{PDF}_{\text{inv}} = \frac{1}{\tau \cdot (\ln(\tau_{\max}) - \ln(\tau_{\min}))}. \quad (3.18)$$

This re-weighting factor is then calculated as

$$w_{\text{lifetime}} = \frac{\text{PDF}_{\text{exp}}}{\text{PDF}_{\text{inv}}} = \frac{\Gamma_{\text{total}}(m_4) \cdot |U_{\tau 4}|^2}{\hbar} \cdot \tau \cdot (\ln(\tau_{\max}) - \ln(\tau_{\min})) \cdot e^{\frac{-\tau}{\tau_{\text{proper}}}}. \quad (3.19)$$

Adding another factor of $|U_{\tau 4}|^2$ to account for the mixing at the interaction vertex the total re-weighting factor becomes

$$w_{\text{total}} = |U_{\tau 4}|^2 \cdot w_{\text{lifetime}}. \quad (3.20)$$

If this additional weighting factor is multiplied to a generation weight (like in Equation ??), the livetime, and the oscillated primary neutrino flux, it results in the number of expected events in the detector for this particular MC event for a chosen mixing (and mass).

add table with number of gen level files? mention the event number is smaller because of kinematic condition?

3.2.4 Generation Level Distributions

Figure 3.6 shows some selected generation level distributions. Additional distributions can be found in Figure A.3.

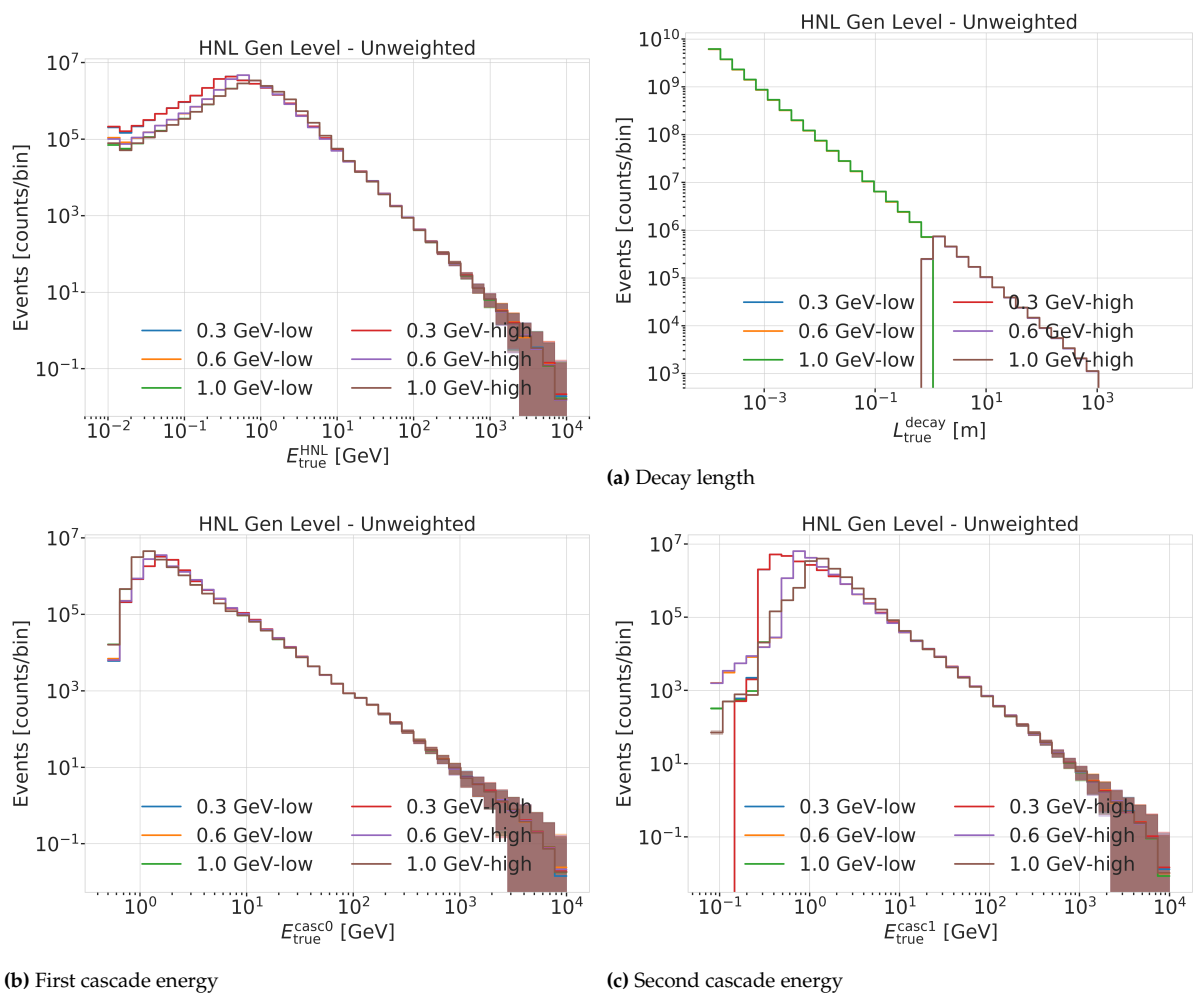


Figure 3.6: Generation level distributions of the model dependent simulation.

APPENDIX

A

Heavy Neutral Lepton Signal Simulation

A.1 Model Independent Simulation Distributions

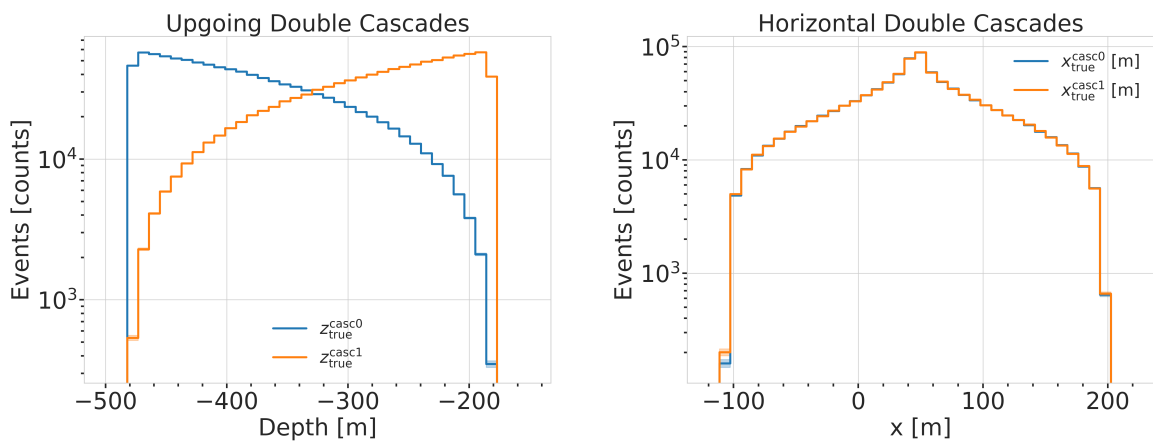


Figure A.1: Generation level distributions of the simplistic simulation sets. Vertical positions (left) and horizontal positions (right) of both sets are shown.

- Re-make plot with x,y for horizontal set one plot!
- Re-make plot with x, y, z for both cascades in one.
- Re-arrange plots in a more sensible way.

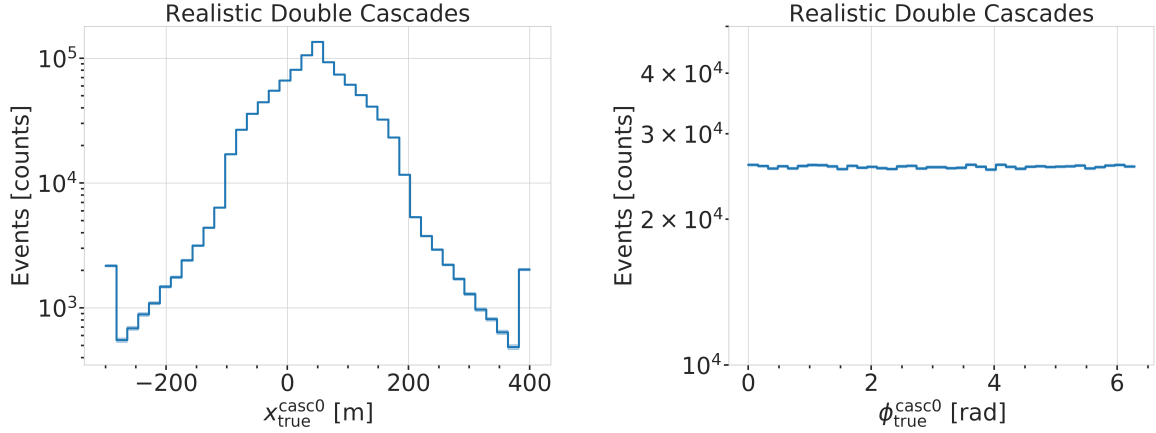


Figure A.2: Generation level distributions of the realistic simulation set. Shown are the cascade x, y, z positions (left) and direction angles (right).

A.2 Model Dependent Simulation Distributions

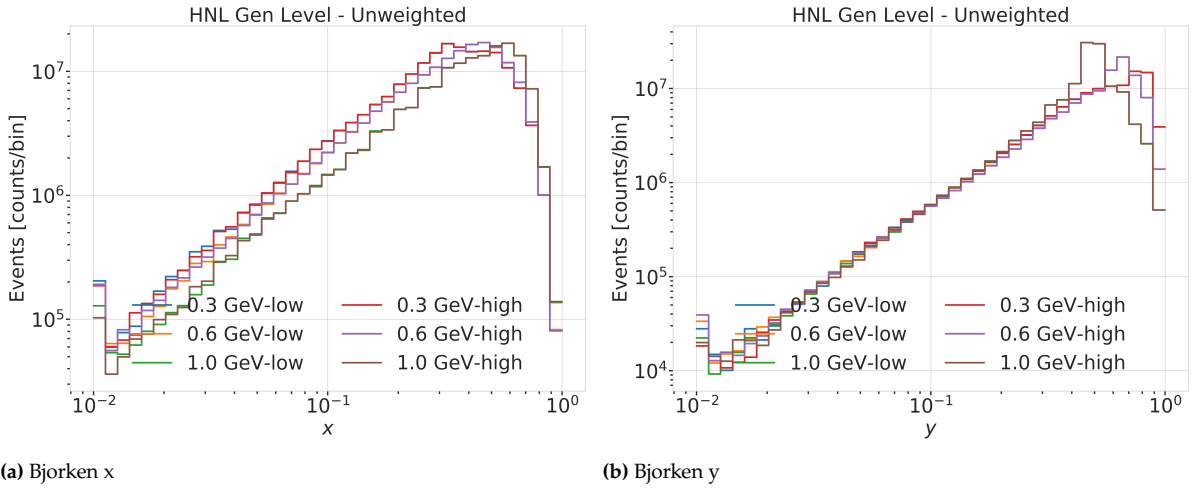


Figure A.3: Generation level distributions of the model dependent simulation.

B

Analysis Checks

B.1 Minimization Robustness

Figure B.1 shows additional Asimov inject/recover tests for the 0.3 GeV and the 1.0 GeV mass sets. The tests were described in Section ??.

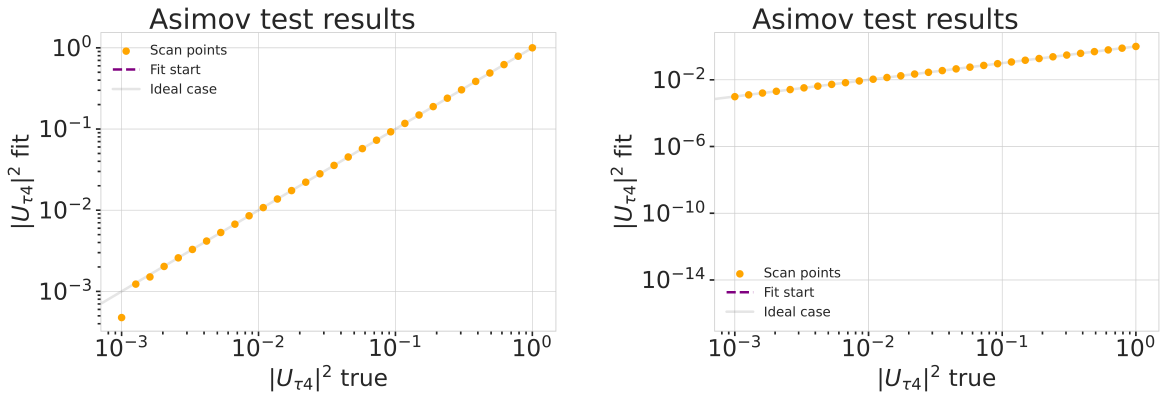


Figure B.1: Asimov inject/recover test for the 0.3 GeV (left) and the 1.0 GeV (right) mass sets. Mixing values between 10^{-3} and 10^0 are injected and fit back with the full analysis chain. The injected parameter is always recovered within the statistical uncertainty.

B.1.1 Ensemble Tests

Figure B.2 shows additional TS distributions from pseudo-data trials and the observed TS from the fit to the data for the ensemble for the 0.3 GeV and the 1.0 GeV mass sets. The tests were described in Section ??.

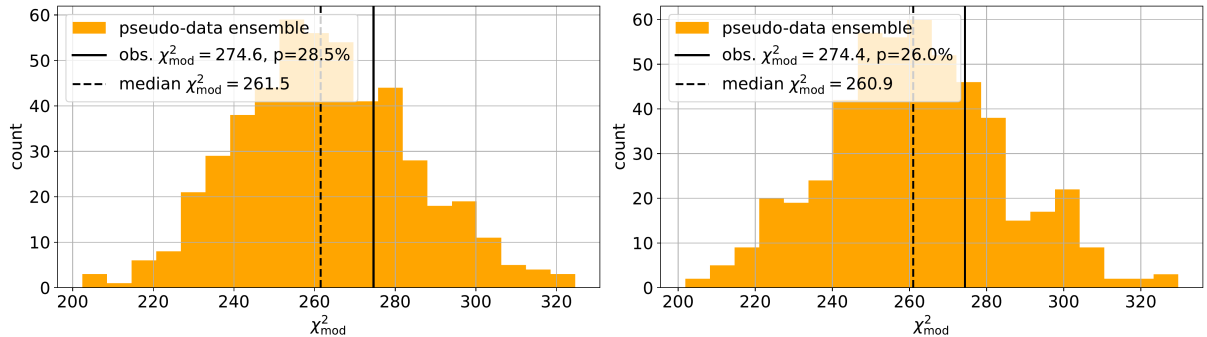


Figure B.2: Observed fit TS and TS distribution from pseudo-data trials for the 0.3 GeV (left) and the 1.0 GeV (right) mass set.

Bibliography

Here are the references in citation order.

- [1] C. N. Yang and R. L. Mills. "Conservation of Isotopic Spin and Isotopic Gauge Invariance". In: *Physical Review* 96.1 (Oct. 1954), pp. 191–195. doi: [10.1103/PhysRev.96.191](https://doi.org/10.1103/PhysRev.96.191) (cited on page 1).
- [2] S. Weinberg. "A Model of Leptons". In: *Phys. Rev. Lett.* 19 (21 Nov. 1967), pp. 1264–1266. doi: [10.1103/PhysRevLett.19.1264](https://doi.org/10.1103/PhysRevLett.19.1264) (cited on page 1).
- [3] S. L. Glashow. "Partial-symmetries of weak interactions". In: *Nuclear Physics* 22.4 (Feb. 1961), pp. 579–588. doi: [10.1016/0029-5582\(61\)90469-2](https://doi.org/10.1016/0029-5582(61)90469-2) (cited on page 1).
- [4] R. Jackiw. "Physical Formulations: Elementary Particle Theory. Relativistic Groups and Analyticity. Proceedings of the eighth Nobel Symposium, Aspenäsgården, Lerum, Sweden, May 1968. Nils Svartholm, Ed. Interscience (Wiley), New York, and Almqvist and Wiksell, Stockholm, 1969. 400 pp., illus. \$31.75." In: *Science* 168.3936 (1970), pp. 1196–1197. doi: [10.1126/science.168.3936.1196.b](https://doi.org/10.1126/science.168.3936.1196.b) (cited on page 1).
- [5] P. Higgs. "Broken symmetries, massless particles and gauge fields". In: *Physics Letters* 12.2 (1964), pp. 132–133. doi: [https://doi.org/10.1016/0031-9163\(64\)91136-9](https://doi.org/10.1016/0031-9163(64)91136-9) (cited on page 1).
- [6] M. Gell-Mann. "A Schematic Model of Baryons and Mesons". In: *Resonance* 24 (1964), pp. 923–925 (cited on page 1).
- [7] G. Zweig. "An SU(3) model for strong interaction symmetry and its breaking. Version 2". In: *DEVELOPMENTS IN THE QUARK THEORY OF HADRONS. VOL. 1. 1964 - 1978*. Ed. by D. B. Lichtenberg and S. P. Rosen. Feb. 1964, pp. 22–101 (cited on page 1).
- [8] D. J. Gross and F. Wilczek. "Ultraviolet Behavior of Non-Abelian Gauge Theories". In: *PRL* 30.26 (June 1973), pp. 1343–1346. doi: [10.1103/PhysRevLett.30.1343](https://doi.org/10.1103/PhysRevLett.30.1343) (cited on page 1).
- [9] C. Giunti and C. W. Kim. *Fundamentals of Neutrino Physics and Astrophysics*. Oxford University Press, Mar. 2007 (cited on page 1).
- [10] M. D. Schwartz. *Quantum Field Theory and the Standard Model*. Cambridge University Press, 2013 (cited on page 1).
- [11] T. Yanagida. "Horizontal Symmetry and Masses of Neutrinos". In: *Progress of Theoretical Physics* 64.3 (Sept. 1980), pp. 1103–1105. doi: [PTP.64.1103](https://doi.org/10.1103/PTP.64.1103) (cited on page 5).
- [12] P. Astier et al. "Search for heavy neutrinos mixing with tau neutrinos". In: *Phys. Lett. B* 506 (2001), pp. 27–38. doi: [10.1016/S0370-2693\(01\)00362-8](https://doi.org/10.1016/S0370-2693(01)00362-8) (cited on page 5).
- [13] R. Acciari et al. "New Constraints on Tau-Coupled Heavy Neutral Leptons with Masses mN=280–970 MeV". In: *Phys. Rev. Lett.* 127.12 (2021), p. 121801. doi: [10.1103/PhysRevLett.127.121801](https://doi.org/10.1103/PhysRevLett.127.121801) (cited on page 5).
- [14] J. Orloff, A. N. Rozanov, and C. Santoni. "Limits on the mixing of tau neutrino to heavy neutrinos". In: *Phys. Lett. B* 550 (2002), pp. 8–15. doi: [10.1016/S0370-2693\(02\)02769-7](https://doi.org/10.1016/S0370-2693(02)02769-7) (cited on page 5).
- [15] I. Boiarska et al. "Blast from the past: constraints from the CHARM experiment on Heavy Neutral Leptons with tau mixing". In: (July 2021) (cited on page 5).
- [16] P. Abreu et al. "Search for neutral heavy leptons produced in Z decays". In: *Z. Phys. C* 74 (1997). [Erratum: *Z.Phys.C* 75, 580 (1997)], pp. 57–71. doi: [10.1007/s002880050370](https://doi.org/10.1007/s002880050370) (cited on page 5).
- [17] P. Coloma et al. "Double-Cascade Events from New Physics in Icecube". In: *Phys. Rev. Lett.* 119.20 (2017), p. 201804. doi: [10.1103/PhysRevLett.119.201804](https://doi.org/10.1103/PhysRevLett.119.201804) (cited on page 6).
- [18] P. Coloma. "Icecube/DeepCore tests for novel explanations of the MiniBooNE anomaly". In: *Eur. Phys. J. C* 79.9 (2019), p. 748. doi: [10.1140/epjc/s10052-019-7256-8](https://doi.org/10.1140/epjc/s10052-019-7256-8) (cited on page 6).

- [19] P. Coloma et al. "GeV-scale neutrinos: interactions with mesons and DUNE sensitivity". In: *Eur. Phys. J. C* 81.1 (2021), p. 78. doi: [10.1140/epjc/s10052-021-08861-y](https://doi.org/10.1140/epjc/s10052-021-08861-y) (cited on pages 6, 8, 9, 28–30).
- [20] M. Thomson. *Modern particle physics*. Cambridge [u.a.]: Cambridge University Press, 2013, XVI, 554 S. (Cited on page 9).
- [21] S. L. Glashow. "Partial-symmetries of weak interactions". In: *Nuclear Physics* 22.4 (1961), pp. 579–588. doi: [https://doi.org/10.1016/0029-5582\(61\)90469-2](https://doi.org/10.1016/0029-5582(61)90469-2) (cited on page 9).
- [22] M. Tanabashi et al. "Review of Particle Physics". In: *Phys. Rev. D* 98 (3 Aug. 2018), p. 030001. doi: [10.1103/PhysRevD.98.030001](https://doi.org/10.1103/PhysRevD.98.030001) (cited on pages 9, 11, 12, 20).
- [23] A. Terliuk. "Measurement of atmospheric neutrino oscillations and search for sterile neutrino mixing with IceCube DeepCore". PhD thesis. Berlin, Germany: Humboldt-Universität zu Berlin, Mathematisch-Naturwissenschaftliche Fakultät, 2018. doi: [10.18452/19304](https://doi.org/10.18452/19304) (cited on pages 9, 11, 21).
- [24] J. A. Formaggio and G. P. Zeller. "From eV to EeV: Neutrino cross sections across energy scales". In: *Rev. Mod. Phys.* 84 (3 Sept. 2012), pp. 1307–1341. doi: [10.1103/RevModPhys.84.1307](https://doi.org/10.1103/RevModPhys.84.1307) (cited on page 10).
- [25] M. Honda et al. "Atmospheric neutrino flux calculation using the NRLMSISE-00 atmospheric model". In: *Phys. Rev. D* 92 (2 July 2015), p. 023004. doi: [10.1103/PhysRevD.92.023004](https://doi.org/10.1103/PhysRevD.92.023004) (cited on pages 11, 12).
- [26] A. Fedynitch et al. "Calculation of conventional and prompt lepton fluxes at very high energy". In: *European Physical Journal Web of Conferences*. Vol. 99. European Physical Journal Web of Conferences. Aug. 2015, p. 08001. doi: [10.1051/epjconf/20159908001](https://doi.org/10.1051/epjconf/20159908001) (cited on page 12).
- [27] M. Honda et al. "Calculation of atmospheric neutrino flux using the interaction model calibrated with atmospheric muon data". In: *Phys. Rev. D* 75 (4 Feb. 2007), p. 043006. doi: [10.1103/PhysRevD.75.043006](https://doi.org/10.1103/PhysRevD.75.043006) (cited on page 12).
- [28] S. Bilenky and B. Pontecorvo. "Lepton mixing and neutrino oscillations". In: *Physics Reports* 41.4 (1978), pp. 225–261. doi: [10.1016/0370-1573\(78\)90095-9](https://doi.org/10.1016/0370-1573(78)90095-9) (cited on page 12).
- [29] P. A. M. Dirac. "The Quantum Theory of the Emission and Absorption of Radiation". In: *Proceedings of the Royal Society of London Series A* 114.767 (Mar. 1927), pp. 243–265. doi: [10.1098/rspa.1927.0039](https://doi.org/10.1098/rspa.1927.0039) (cited on page 13).
- [30] M. G. Aartsen et al. "The IceCube Neutrino Observatory: instrumentation and online systems". In: *Journal of Instrumentation* 12.3 (Mar. 2017), P03012. doi: [10.1088/1748-0221/12/03/P03012](https://doi.org/10.1088/1748-0221/12/03/P03012) (cited on pages 15, 17).
- [31] P. B. Price, K. Woschnagg, and D. Chirkin. "Age vs depth of glacial ice at South Pole". In: *Geophysical Research Letters* 27.14 (2000), pp. 2129–2132. doi: <https://doi.org/10.1029/2000GL011351> (cited on page 16).
- [32] R. Abbasi et al. "In-situ estimation of ice crystal properties at the South Pole using LED calibration data from the IceCube Neutrino Observatory". In: *The Cryosphere Discussions* 2022 (2022), pp. 1–48. doi: [10.5194/tc-2022-174](https://doi.org/10.5194/tc-2022-174) (cited on page 16).
- [33] R. Abbasi et al. "The IceCube data acquisition system: Signal capture, digitization, and timestamping". In: *Nuclear Instruments and Methods in Physics Research Section A: Accelerators, Spectrometers, Detectors and Associated Equipment* 601.3 (2009), pp. 294–316. doi: <https://doi.org/10.1016/j.nima.2009.01.001> (cited on pages 16, 17).
- [34] M. G. Aartsen et al. "Energy Reconstruction Methods in the IceCube Neutrino Telescope". In: *JINST* 9 (2014), P03009. doi: [10.1088/1748-0221/9/03/P03009](https://doi.org/10.1088/1748-0221/9/03/P03009) (cited on page 17).
- [35] J. Feintzeig. "Searches for Point-like Sources of Astrophysical Neutrinos with the IceCube Neutrino Observatory". PhD thesis. University of Wisconsin, Madison, Jan. 2014 (cited on page 17).
- [36] N. Kulacz. "In Situ Measurement of the IceCube DOM Efficiency Factor Using Atmospheric Minimum Ionizing Muons". MA thesis. University of Alberta, 2019 (cited on page 17).
- [37] R. Abbasi et al. "The design and performance of IceCube DeepCore". In: *Astropart. Phys.* 35.10 (2012), pp. 615–624. doi: [10.1016/j.astropartphys.2012.01.004](https://doi.org/10.1016/j.astropartphys.2012.01.004) (cited on page 17).

- [38] P. A. Cherenkov. "Visible Radiation Produced by Electrons Moving in a Medium with Velocities Exceeding that of Light". In: *Phys. Rev.* 52 (4 Aug. 1937), pp. 378–379. doi: [10.1103/PhysRev.52.378](https://doi.org/10.1103/PhysRev.52.378) (cited on page 18).
- [39] I. Frank and I. Tamm. "Coherent visible radiation from fast electrons passing through matter". In: *C. R. Acad. Sci. USSR* 14 (1937), pp. 109–114 (cited on page 19).
- [40] I. Tamm. "Radiation Emitted by Uniformly Moving Electrons". In: *Selected Papers*. Ed. by B. M. Bolotovskii, V. Y. Frenkel, and R. Peierls. Berlin, Heidelberg: Springer Berlin Heidelberg, 1991, pp. 37–53. doi: [10.1007/978-3-642-74626-0_3](https://doi.org/10.1007/978-3-642-74626-0_3) (cited on page 19).
- [41] L. Rädel and C. Wiebusch. "Calculation of the Cherenkov light yield from low energetic secondary particles accompanying high-energy muons in ice and water with Geant4 simulations". In: *Astroparticle Physics* 38 (Oct. 2012), pp. 53–67. doi: [10.1016/j.astropartphys.2012.09.008](https://doi.org/10.1016/j.astropartphys.2012.09.008) (cited on page 19).
- [42] D. Chirkin and W. Rhode. "Propagating leptons through matter with Muon Monte Carlo (MMC)". In: (July 2004) (cited on page 19).
- [43] L. Raedel. "Simulation Studies of the Cherenkov Light Yield from Relativistic Particles in High-Energy Neutrino Telescopes with Geant4". MA thesis. Aachen, Germany: Rheinisch-Westfälischen Technischen Hochschule, 2012 (cited on pages 19, 20).
- [44] S. Agostinelli et al. "Geant4—a simulation toolkit". In: *Nucl. Instr. Meth. Phys. Res.* 506.3 (July 2003), pp. 250–303. doi: [10.1016/s0168-9002\(03\)01368-8](https://doi.org/10.1016/s0168-9002(03)01368-8) (cited on page 20).
- [45] T. Gabriel et al. "Energy dependence of hadronic activity". In: *Nuclear Instruments and Methods in Physics Research Section A: Accelerators, Spectrometers, Detectors and Associated Equipment* 338.2 (1994), pp. 336–347. doi: [https://doi.org/10.1016/0168-9002\(94\)91317-X](https://doi.org/10.1016/0168-9002(94)91317-X) (cited on page 20).
- [46] G. Van Rossum and F. L. Drake. *Python 3 Reference Manual*. Scotts Valley, CA: CreateSpace, 2009 (cited on page 23).
- [47] R. Abbasi et al. "LeptonInjector and LeptonWeighter: A neutrino event generator and weighter for neutrino observatories". In: *Comput. Phys. Commun.* 266 (2021), p. 108018. doi: [10.1016/j.cpc.2021.108018](https://doi.org/10.1016/j.cpc.2021.108018) (cited on page 27).
- [48] J. Alwall et al. "The automated computation of tree-level and next-to-leading order differential cross sections, and their matching to parton shower simulations". In: *JHEP* 07 (2014), p. 079. doi: [10.1007/JHEP07\(2014\)079](https://doi.org/10.1007/JHEP07(2014)079) (cited on page 28).
- [49] C. Argüelles. <https://github.com/arguelles/NuXSp\lMkr> (cited on page 28).
- [50] J.-M. Levy. "Cross-section and polarization of neutrino-produced tau's made simple". In: *J. Phys. G* 36 (2009), p. 055002. doi: [10.1088/0954-3899/36/5/055002](https://doi.org/10.1088/0954-3899/36/5/055002) (cited on page 28).
- [51] E. Tiesinga et al. "CODATA recommended values of the fundamental physical constants: 2018". In: *Rev. Mod. Phys.* 93 (2 July 2021), p. 025010. doi: [10.1103/RevModPhys.93.025010](https://doi.org/10.1103/RevModPhys.93.025010) (cited on page 30).